iScience

CellPress
OPEN ACCESS

Article

Conditional deletion of LRRC8A in the brain reduces stroke damage independently of swelling-activated glutamate release

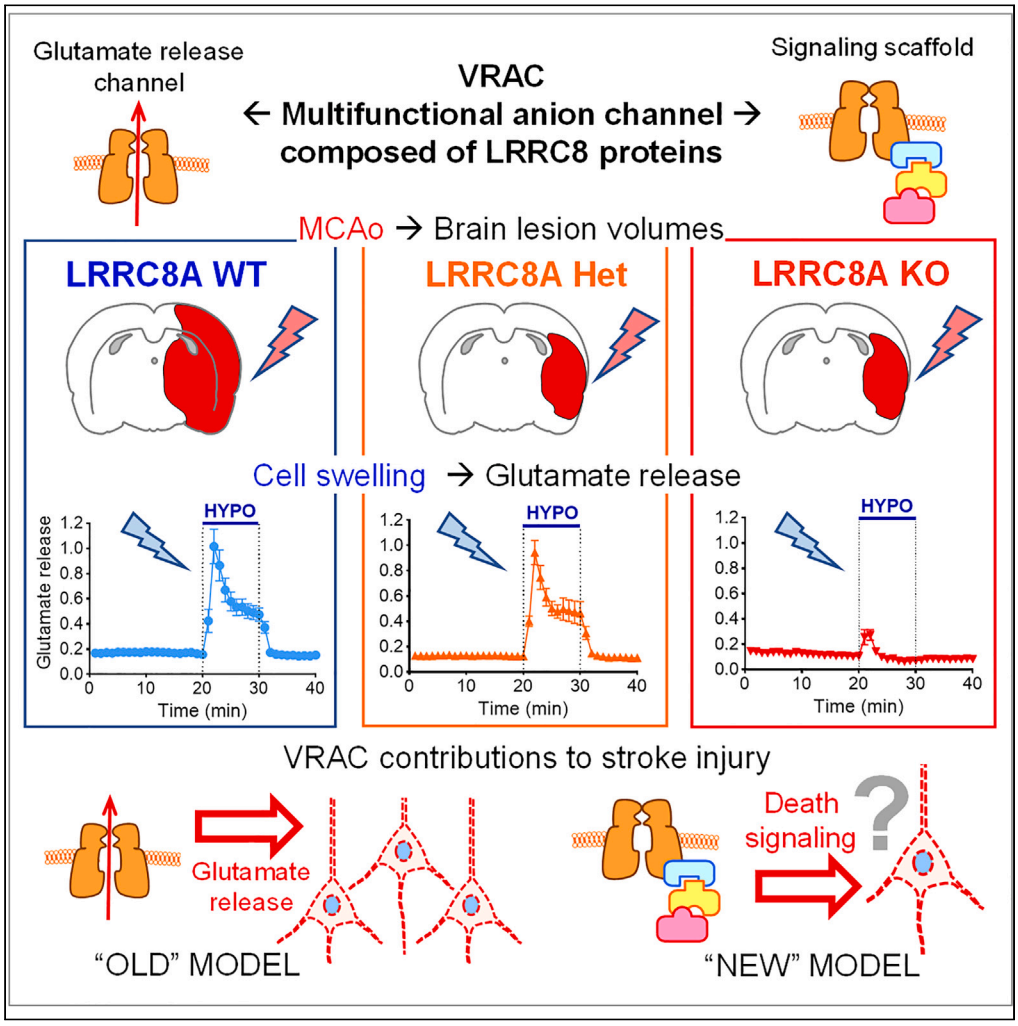

Mustafa Balkaya, Preeti Dohare, Sophie Chen, ..., Julia W. Nalwalk, Rajan Sah, Alexander A. Mongin

mongina@amc.edu

Highlights

Glutamate release via VRAC channels is thought to drive brain injury in stroke

Full and heterozygous loss of the VRAC protein LRRC8A equally reduces stroke damage

Swelling-activated glutamate release via VRAC is lost in LRRC8A KO but not Het mice

The mechanism behind VRAC involvement in stroke injury must be revisited

Balkaya et al., iScience 26, 106669
May 19, 2023
https://doi.org/10.1016/j.isci.2023.106669

iScience

CellPress
OPEN ACCESS

Article

Conditional deletion of LRRC8A in the brain reduces stroke damage independently of swelling-activated glutamate release

Mustafa Balkaya,[1] Preeti Dohare,[1] Sophie Chen,[1] Alexandra L. Schober,[1,3] Antonio M. Fidaleo,[1] Julia W. Nalwalk,[1] Rajan Sah,[2] and Alexander A. Mongin[1,4,*]

SUMMARY

The ubiquitous volume-regulated anion channels (VRACs) facilitate cell volume control and contribute to many other physiological processes. Treatment with non-specific VRAC blockers or brain-specific deletion of the essential VRAC subunit LRRC8A is highly protective in rodent models of stroke. Here, we tested the widely accepted idea that the harmful effects of VRACs are mediated by release of the excitatory neurotransmitter glutamate. We produced conditional LRRC8A knockout either exclusively in astrocytes or in the majority of brain cells. Genetically modified mice were subjected to an experimental stroke (middle cerebral artery occlusion). The astrocytic LRRC8A knockout yielded no protection. Conversely, the brain-wide LRRC8A deletion strongly reduced cerebral infarction in both heterozygous (Het) and full KO mice. Yet, despite identical protection, Het mice had full swelling-activated glutamate release, whereas KO animals showed its virtual absence. These findings suggest that LRRC8A contributes to ischemic brain injury via a mechanism other than VRAC-mediated glutamate release.

INTRODUCTION

Stroke is defined as a loss of brain functions caused by an interruption of cerebral blood flow, either because of vessel occlusion (ischemic stroke) or rupture (hemorrhagic stroke).[1,2] The high prevalence, rapid onset, and severity of tissue injury make stroke the second leading cause of death and the third leading source of disability worldwide.[2,3] Despite the large burden on public health, the currently approved acute stroke therapies are limited to thrombolytic agents, most notably tissue plasminogen activator (tPA or Alteplase) and its genetically modified form tenecteplase, or mechanical retrieval of clots.[2] Despite many promising preclinical studies, clinical trials have failed to confirm efficacy of neuroprotective agents in stroke patients.[4,5] Therefore, there is a pressing need for a better understanding of stroke pathology and the discovery of new therapeutic targets.

One prospective molecular target in stroke that gained attention over the past two decades is the volume-regulated anion channels (VRACs). VRACs are the ubiquitous chloride channels, which are activated in response to cellular swelling and play a canonical role in cell volume regulation.[6–8] Opening of VRACs initiates efflux of cytosolic anions, indirectly facilitating the loss of intracellular K^+ and osmotically obligated water.[9–11] In addition to inorganic anions, such as Cl^- and bicarbonate, VRACs are permeable to various small organic molecules which carry either a negative charge, such as glutamate, aspartate, lactate, and pyruvate, or are net-neutral, e.g., taurine, sorbitol, glutamine, and GABA.[6–8] Because many amino acid neurotransmitters can permeate VRACs, in the brain their opening can result in hyperexcitability and, in extreme cases, lead to tissue injury.[12–14]

The idea of VRAC contributions to stroke pathology stems from the observations that brain ischemia triggers robust cellular swelling and that swollen cells release large quantities of glutamate [reviewed in[13,15]]. This hypothesis has been tested using pharmacological agents, such as the estrogen receptor antagonist tamoxifen and the more selective DCPIB, which at micromolar levels potently inhibits VRAC. In rodent stroke models, tamoxifen and DCPIB decrease the intraischemic buildup of glutamate and aspartate,[16–18] and potently reduce infarction volumes and neurological deficits.[19–22] Yet, because of possible off-target

[1]Department of Neuroscience and Experimental Therapeutics, Albany Medical College, Albany, NY 12208, USA

[2]Department of Internal Medicine, Washington University School of Medicine, St. Louis, MO 63110, USA

[3]Present address: Department of Neurology and Neurosurgery, Centre for Research in Neuroscience, Research Institute of McGill University Health Centre, Montreal, QC, Canada

[4]Lead contact

*Correspondence: mongina@amc.edu

https://doi.org/10.1016/j.isci.2023.106669

effects of both agents, the specific contribution of VRACs to ischemic pathology remains unresolved. Recently, the field was revolutionized by the discovery that VRACs are comprised of proteins belonging to the Leucine-Rich Repeat-Containing family 8 (LRCC8).[23,24] There are five LRRC8 proteins (LRRC8A-E). LRRC8A is essential for VRAC conductance but must be combined with other LRRC8 homologues to form a diversity of fully functional heterohexameric LRRC8 channels.[23–28] It is now possible to use molecular genetics to definitively test biological roles for the LRRC8A subunit and VRACs.

Our present work follows two recent publications probing the role of LRRC8A in ischemic brain injury. The first study has found that astrocyte-specific LRRC8A knockout moderately reduces brain damage in a murine stroke.[29] A subsequent report revealed more robust protection in mice carrying the brainwide LRRC8A deletion.[30] These discoveries have strengthened the hypothesis that VRAC is an important player in stroke pathology. Yet, such a conclusion is based on a correlation between LRRC8A expression and stroke outcomes without probing the underlying mechanisms and LRRC8A involvement in pathological glutamate release. Another caveat is that conditional knockouts can lead to developmental adaptations. Indeed, the brainwide LRRC8A deletion produces reactive astrogliosis, gives rise to spontaneous seizures, and results in 100% animal mortality within the first eight weeks of postnatal development.[30,31] Therefore, in the present work, to avoid developmental compensation we tested the impact of LRRC8A deletion on stroke outcomes using inducible deletion of LRRC8A in astrocytes. Because astrocytic ablation was not neuroprotective, we extended our efforts to the conditional brain-wide LRRC8A knockout. Surprisingly, our work revealed a lack of correlation between swelling-activated glutamate release and stroke protection.

RESULTS

Validation of *Aldh1l1*^{CreERT2}-driven excision of *Lrrc8a* in the CNS astrocytes

To produce inducible, astrocyte-specific deletion of LRRC8A, we utilized commercially available *Aldh1l1*^{CreERT2} mice, which were produced and validated by the Khakh Laboratory.[32] Aldehyde dehydrogenase 1 family member L1 (ALDH1L1) is a folate metabolism enzyme, whose expression in the adult brain is nearly exclusive to astrocytes.[33] Our breeding strategy yielded the *Aldh1l1*$^{CreERT2/+}$; *Lrrc8a*$^{fl/fl}$ genotype, hereafter referred to as the inducible astrocytic LRRC8A knockout (iaLRRC8A KO) and *Lrrc8a*$^{fl/fl}$ littermates (Figure 1A). Mice were treated with tamoxifen to induce Cre expression or corn oil to provide vehicle treatment control. Altogether, we analyzed four genotype/treatment groups with only one of them carrying the deletion of LRRC8A in astrocytes (Figure 1A). Possible effects of the genotype-independent toxicity were reduced through performing functional assays at 10+ days after tamoxifen induction, at which time tamoxifen and all its metabolites are cleared from the body and the brain.[34]

To validate effective LRRC8A deletion we performed two types of experiments. First, we utilized the inbred tdTomato reporter to visualize Cre activity in the brain. As seen in Figure 1B, tamoxifen treatment of iaLRRC8A KO mice produced robust tdTomato expression throughout the brain. In contrast, no tdTomato fluorescence was observed in the iaLRRC8A KO mice treated with corn oil, except for a few positive cells reflecting spontaneous Cre activation (Figures 1B, 1C, and1D). The *Lrrc8a*$^{fl/fl}$ controls had no tdTomato fluorescence (data not shown). Higher magnification images demonstrated that tdTomato fluorescence overlapped with the astrocytic markers GFAP in hippocampus (Figure 1C) and glutamine synthetase in cortical regions (Figure 1D). We used glutamine synthetase in cortex because of known low GFAP expression levels in this brain region (see Figure 1B and review[35]). Extensive quantification in six brains demonstrated Cre induction in >98% of hippocampal astrocytes and >90% of cortical astrocytes (Figure 1E).

To substantiate LRRC8A protein deletion, we next performed semi-quantitative western blot analyses in whole-brain lysates. We found ~20% reduction of LRRC8A expression in the tamoxifen-treated iaLRRC8A KO mice, as compared to oil-treated iaLRRC8A KO group and tamoxifen-treated *Lrrc8a*$^{fl/fl}$ controls ($p<0.05$, Figures 1F and 1G; primary images in Figure S1). Previously, we found that the brain-wide deletion of LRRC8A reduced astrocytic expression of the glutamate transporter GLT-1.[31] Therefore, we additionally explored if there were changes in GLT-1 immunoreactivity in the iaLRRC8A KO but no differences were detected in any of the tested groups (Figures 1H and 1I; primary images in Figure S2).

Next, to assess the extent of LRRC8A loss in astrocytes, we performed studies in primary astrocyte cultures prepared from neonatal iaLRRC8A KO brains. Astrocyte cultures were treated with either 2 μM hydroxytamoxifen (4-OHT) or vehicle (0.05% DMSO) for 4–14 days and analyzed for the expression levels of LRRC8A and induction of the Cre reporter, tdTomato. tdTomato reporter was expressed as early as

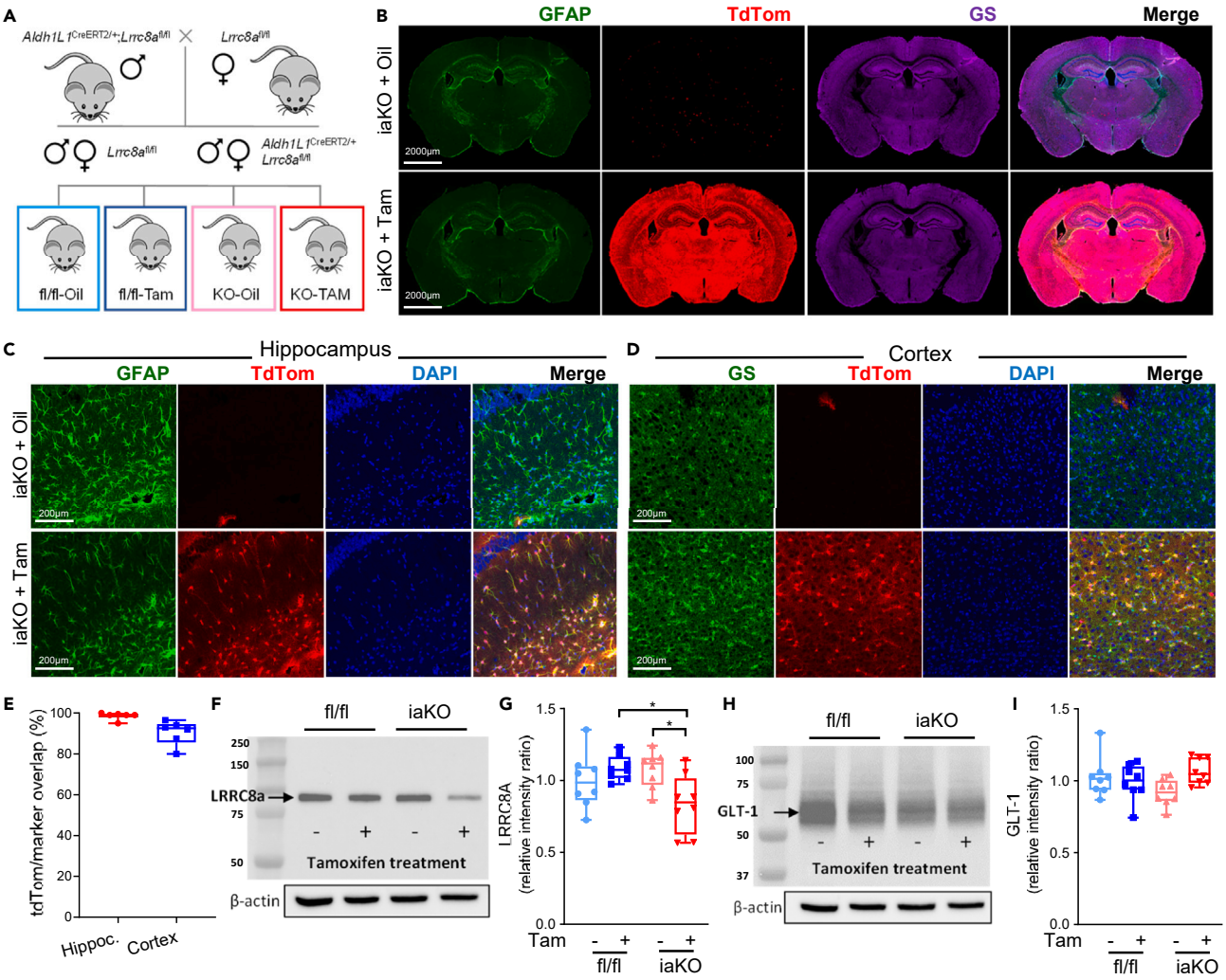

Figure 1. Validation of *Aldh1l1*^{CreERT2} driven LRRC8A deletion in mouse astrocytes *in vivo*

(A) Breeding and treatment strategy for the astrocyte-specific inducible deletion of LRRC8A using *Aldh1l1*^{Cre}-targeted excision of *Lrrc8a*$^{fl/fl}$. The *Aldh1l1*^{CreERT2};*Lrrc8a*$^{fl/fl}$ mice (iaKO) and *Lrrc8a*$^{fl/fl}$ (fl/fl) controls were treated with either tamoxifen (Tam, activates CreERT2) or vehicle (Oil) to generate four experimental groups.

(B) Representative immunohistochemistry images of whole-brain sections from 12-week-old iaKO mice showing expression of the Cre reporter tdTomato (red) and the astrocyte markers, GFAP (green) and glutamine synthetase (GS, purple). Scale bar = 2000 μm.

(C) Representative high magnification images (200×) visualizing the co-expression of tdTomato (red) and GFAP (green) in the hippocampus. Scale bar = 200 μm.

(D) Representative high magnification images (200×) visualizing the co-expression of tdTomato (red) and GS (green) in the cortex. Scale bar = 200 μm.

(E) Quantification of the co-localization of the immunoreactivity (IR) for the Cre reporter tdTomato and the astrocytic markers GFAP (in hippocampus) and GS (Cortex). Data are the mean values ±SD in six brains.

(F) Representative western blot image of LRRC8A expression in the whole brain lysates from four genotype/treatment groups.

(G) Quantification of LRRC8A expression. The boxplot of individual IR values, normalized to β-actin loading and averaged within a set. n = 8/group. *p<0.05, iaKO+Tam vs. fl/fl+Tam and iaKo+oil; two-way ANOVA with Sidak's multiple comparisons test; ##p<0.01, genotype-treatment interaction.

(H) Representative western blot image of GLT1 expression in four genotype/treatment groups.

(I) Quantification of GLT1 expression. The boxplot of individual IR values, normalized to β-actin loading and averaged within a set.

24 h, labeled >70% of cultured cells by days 3–4, and reached saturated intensity by days 6–8 (Figure 2A). Western blot analysis identified robust downregulation of LRRC8A protein expression, with a surprising lag of approximately 10 days (Figures 2B and 2C). The extent of LRRC8A deletion varied among cell preparations from nearly full (representative blot in Figure 2B) to partial, but on average reached ~80% by days 12 and 14 (Figure 2C). The temporal mismatch between changes in LRRC8A and tdTomato expression may indicate the different accessibility of these two genes for Cre.

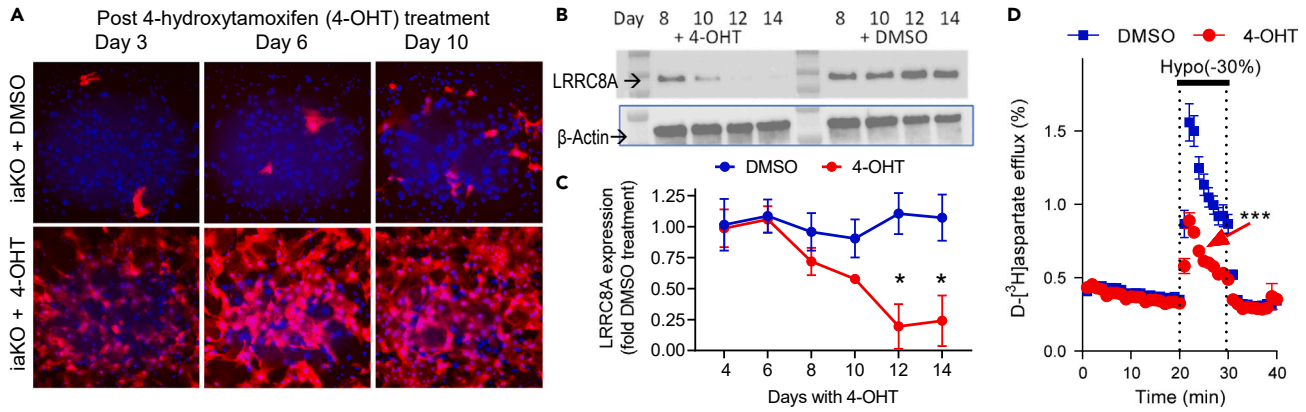

Figure 2. *Aldh1l1*^{CreERT2}-driven reductions in LRRC8A expression and VRAC activity in mouse iaLRRC8A KO astrocytes *in vitro*

(A) Representative images of the Cre reporter tdTomato expression in the *Aldh1l1*^{CreERT2};*Lrrc8a*$^{fl/fl}$ (iaKO) astrocyte cell cultures treated with either 2 μM 4-hydroxytamoxifen (4-OHT) or vehicle control (DMSO). Images show overlay of tdTomato (red) and Hoechst (blue) staining at days 3, 6 and 10 after initiation of treatment.

(B) Representative western blot of LRRC8A expression in 4-OHT of vehicle (DMSO) treated astrocytic cultures at days 8–14 after initiation of treatment.

(C) Quantification of LRRC8A expression. Data are the mean IR values of individual immunoreactivity ±SEM normalized to β-actin loading controls and to average values. n = 3/group. $p<0.05$, 4-OHT vs. DMSO at D12 and D14. Repeated measures ANOVA with Sidak's posthoc comparison.

(D) Quantification of VRAC activity in primary astrocyte cultures, measured as swelling-activated D-[^{3}H]aspartate release. Data are the mean values ±SEM. n = 9 experiments/group performed in three independent cell cultures. ***$p<0.001$, 4-OHT vs. DMSO, The effect of time, treatment, and interaction, repeated measures ANOVA.

Finally, to confirm functional loss of VRAC activity, we employed a radiotracer assay, measuring swelling-activated release of the non-metabolizable glutamate analog, D-[^{3}H]aspartate. This assay, which has been thoroughly validated using RNAi and pharmacological tools, quantifies the activity of the LRRC8A-containing VRAC in large populations of astrocytes and gives comparable results to electrophysiological recordings of VRAC Cl^- currents.[31,36,37] Hypoosmotic challenge of cultured astrocytes stimulated glutamate (D-[^{3}H]aspartate) release via VRAC, and such release was reduced by approximately 70% in the tamoxifen-treated iaLRRC8A KO cultures as compared to the DMSO-treated controls from the same genotype (Figure 2D). Taken together, the results of our *in vivo* and *in vitro* experiments suggest that we successfully downregulated LRRC8A expression in brain astrocytes and that such downregulation was associated with a significant loss of VRAC activity.

Astrocytic LRRC8A deletion does not confer neuroprotection in an MCAo stroke model

We started with four genotype/treatment groups containing mice of both sexes. Either *Lrrc8a*$^{fl/fl}$ controls or iaLRRC8A KO animals were treated with oil or tamoxifen (see group design in Figure 1A). Because tamoxifen is neuroprotective in stroke, ischemia surgeries were performed 10 to 12 days after the final tamoxifen injection, allowing the drug and its metabolites to be cleared from the brain.[34] Mice were subjected to 40-min occlusion of the middle cerebral artery (MCAo) to investigate potential beneficial effects of eliminating LRRC8A and VRAC in astrocytes (for transparent animal use reporting see Figure S3). Mice were allowed to survive for 72 h during which time they were evaluated for neurological deficits, followed by quantification of stroke infarction volumes using TTC staining. Because stroke outcomes are significantly impacted by intra- and postischemic variations in blood flow,[38] we extensively analyzed cerebral blood flow dynamics in real time during the whole MCAo procedure and throughout the first 10 min of reperfusion using a Laser Doppler flowmetry (Figure 3A). The laser Doppler probe was placed in the infarction core territory and the signal was averaged across predetermined 2-min time bins as shown. Averaging the signal helped to reduce variability because of small spontaneous vessel relaxations and contractions, which can be seen in a representative graph (Figure 3A). Two-way ANOVA analysis revealed no significant difference among groups immediately after MCAo or near the end of the ischemic episode (Figures 3B and 3C), suggesting similar ischemia severity in all groups. Furthermore, we found no variations in reperfusion rates among all four tested groups (Figure 3D).

Our pre-planned primary endpoint was brain lesion size analyzed at 72 h post-ischemia. In this study, 40-min MCAo produced large infarction volumes in striatal and cortical regions, in line with previous

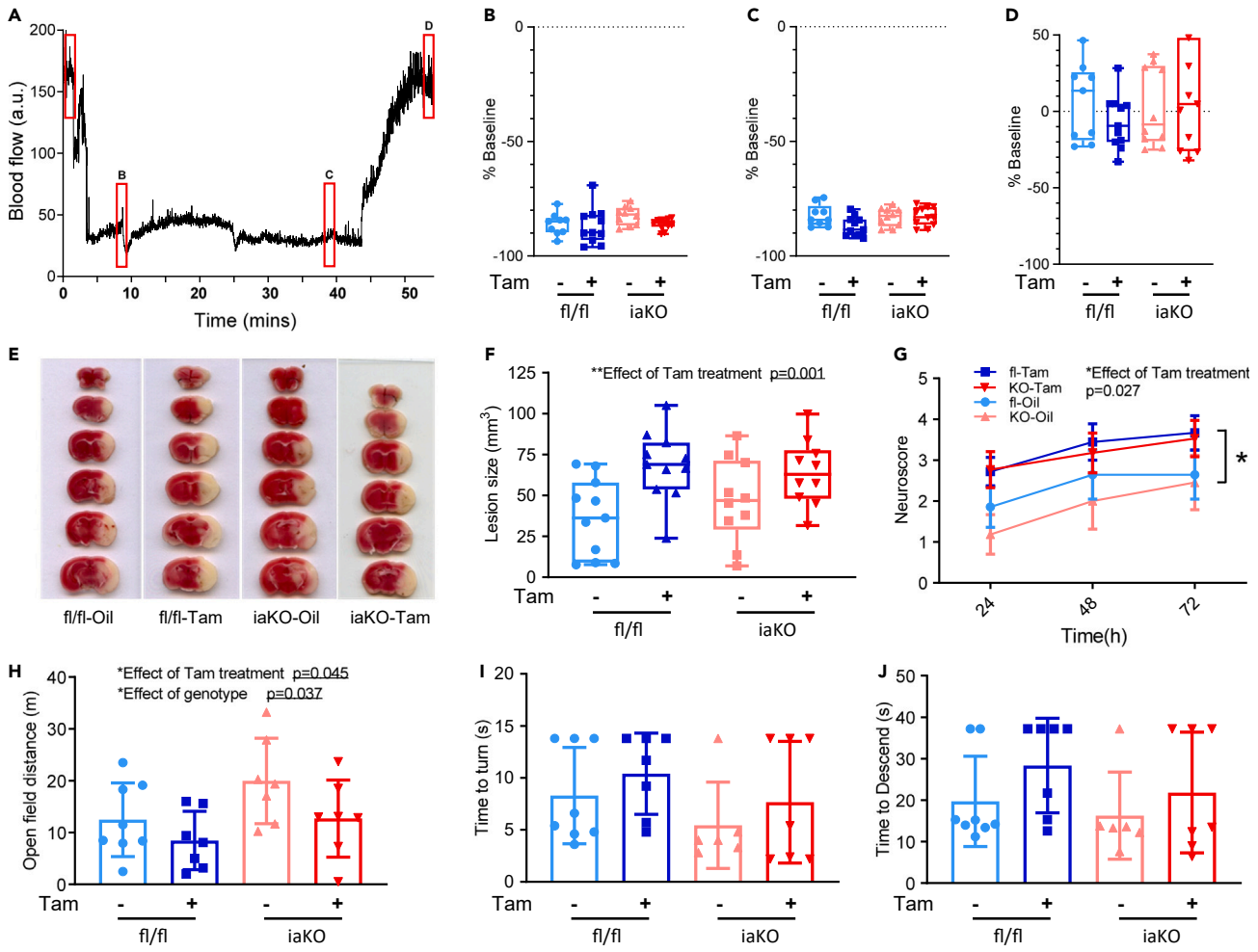

Figure 3. Effects of inducible astrocytic LRRC8A knockout (iaLRRC8A KO) on physiological parameters and outcomes in murine experimental stroke

(A) Representative chart from a single animal of the cerebral blood flow dynamics in experimental stroke as measured with a laser Doppler (LD) flowmetry. Cerebral ischemia was induced via occlusion of the middle cerebral artery (MCAo). Red boxes indicate the 2-min intervals used for quantitative analyses of blood perfusion levels.

(B) The boxplot graph of the post-occlusion blood flow rates in mice from four genotype/treatment groups (indicated by 'B' in the representative graph). n = 9–11/group.

(C) The boxplot graph of the pre-reperfusion blood flow levels ('C'). n = 9–11/group.

(D) The boxplot graph of the blood flow recovery during initial reperfusion ('D'). n = 9–11/group.

(E) Representative TTC staining images of MCAo lesion volumes in four genotype/treatment groups at 72-h post-stroke.

(F) Boxplot graph of quantitative analysis of MCAo infarction volumes in four experimental groups. *Only the effect of tamoxifen treatment has been found; p = 0.001, two-way ANOVA. N = 10–11.

(G) Neurological deficits in four experimental groups assessed daily over 72 h using the neuroscore test. *Only the effect of tamoxifen treatment has been found; repeated measures ANOVA.

(H) Comparison of spontaneous locomotor activity among groups as assessed by total distance traveled in the open field test. Mean values ±SD. N = 7–8. *p<0.05, effect of treatment and genotype; two-way ANOVA.

(I) Lack of effect of treatment and genotype on time to perform a full turn in the pole test. Mean values ±SD. N = 6–8.

(J) Lack of effect of treatment and genotype on time to descend in the pole test. Mean values ±SD. N = 6–8.

findings in this model [Figure 3E and refs.[39,40]]. Two-way ANOVA of brain lesion sizes did not reveal any effect of genotype or interaction between genotype and treatment (Figure 3F; all primary images in Figures S4 and S5). Pre-planned post-hoc analysis did not reveal differences between sexes (data not shown). These findings strongly suggest that this strategy of astrocytic LRRC8A deletion is not neuroprotective. Unexpectedly, there was a statistically significant worsening of stroke outcomes after tamoxifen

treatment in both genotypes (p = 0.001, Figure 3F). The latter finding likely indicates that animals had not fully recovered from genotype-independent tamoxifen toxicity, even 10-12-day after the last tamoxifen injection. Overall, we saw no evidence for protection by the astrocyte-specific LRRC8A deletion.

Pre-planned secondary outcomes included post-MCAo mortality and several behavioral assessments of neurological deficits. We found no effect of genotype or genotype-treatment interaction on death rates (data not shown). Our additional secondary endpoint was a neurological deficit score on a five-point scale, which was assessed for 3 consecutive days after MCAo. We found no effect of genotype or genotype-treatment interaction (Figure 3G). However, on its own, tamoxifen treatment worsened the stroke-induced deficits in a genotype-independent manner (p = 0.027, Figure 3G). This was consistent with larger infarctions and reflected the trend for higher mortality in the two tamoxifen-treated groups.

We next quantified post-stroke deficits using two sensitive behavioral techniques, the open field test, and the pole test, which are commonly employed by the field. The open field test assesses changes in spontaneous activity and anxiety.[41] The pole test is a sensitive measure of simple motor functions, grip strength, and coordination.[41] In the open field test, two-way ANOVA did not reveal an effect of genotype or an interaction between treatment and genotype (Figure 3H), corresponding to an absence of beneficial effect of astrocytic LRRC8A deletion. However, yet again, we found the genotype-independent negative effect of tamoxifen on spontaneous mobility (p = 0.045, Figure 3H). In the pole test, two-way ANOVA found no effect of genotype, treatment or treatment-genotype interaction on *time-to-turn* (Figure 3I) and *time-to-descend* parameters (Figure 3G). Overall, behavioral tests were consistent with histological outcomes and showed no protection by LRRC8A deletion in astrocytes.

Nestin^{Cre}-driven deletion of *Lrrc8a* eliminates LRRC8A protein in the brain

The failure to detect histological or behavioral benefits of the astrocyte-specific LRRC8A deletion in stroke, prompted us to re-evaluate the previously reported neuroprotective effects of the brain-wide conditional LRRC8A knockout using *Nestin*^{Cre}-driven gene excision. The latter genetic strategy was reported to reduce stroke infarction volumes in LRRC8A-null mice by at least 50%.[30]

The *Nestin*^{Cre} knockout strategy allows for effective excision of floxed product(s) in all types of brain neuroectodermal cells, including astrocytes, oligodendrocytes and neurons.[42] Nestin is a type VI intermediate filament protein that is abundant in neuronal stem cells throughout development and adulthood; it is expressed in developing mouse embryos as early as E7.5.[43] Complete elimination of LRRC8A in the brain using the *Nestin*^{Cre} strategy has been extensively validated in our recent work.[31] In the present study, we used the same breeding strategy (Figure 4A) and additionally used Ai14 tdTomato reporter to ensure that there is no non-specific germline recombination. Our breeding produced four genotypes: control *Lrrc8a*$^{fl/+}$ (containing one wild-type *Lrrc8a* allele; abbreviated fl/+), control *Lrrc8a*$^{fl/fl}$ (fl/fl), heterozygous deletion (*Nestin*^{Cre};*Lrrc8a*$^{fl/+}$, Het), and the full LRRC8A brain knockout (*Nestin*^{Cre};*Lrrc8a*$^{fl/fl}$, hereafter referred to as bLRRC8A KO). We used both sexes of all four genotypes for evaluating the role of LRRC8A protein and VRAC in stroke outcomes.

Much like in our prior work[31] and the study by Zhou et al.,[30] bLRRC8A KO mice developed normally but showed spontaneous mortality beginning week 5 with majority of animals dead by week 9. Our prior study established that the main cause of death during adolescence was spontaneous seizure.[31] Because of mortality and animal size limitations, we had to perform the MCAo procedure at 6–6.5 weeks of age, by which time ~33% of born bLRRC8A KO animals were already lost (Figure 4B). To ensure that LRRC8A is deleted in the present cohort of animals, we performed semi-quantitative western blotting in brain lysates from all four genotypes. Consistent with our prior work,[31] we found complete loss of LRRC8A immunoreactivity in bLRRC8A KO animals (Figures 4C and 4D; primary images in Figure S6). Het brains demonstrated ~40% reduction in LRRC8A levels (Figures 4C and 4D). Of interest, in fl/fl specimens LRRC8A expression was also reduced by 20% as compared to fl/+ tissue (p = 0.093; Figures 4C and 4D). Although the latter reduction was only a trend, it matched the findings of our prior study, which were statistically significant.[31] This phenomenon likely indicates that introduction of *loxP* sites changes mRNA stability or translation efficacy.

In addition, we analyzed the expression levels of astrocytic glutamate transporter GLT1. This is important because decreases in GLT1-dependent glutamate buffering may impact stroke outcomes[44,45] and we have previously found that the loss of LRRC8A is associated with a partial loss of GLT-1.[31] In the present cohort of

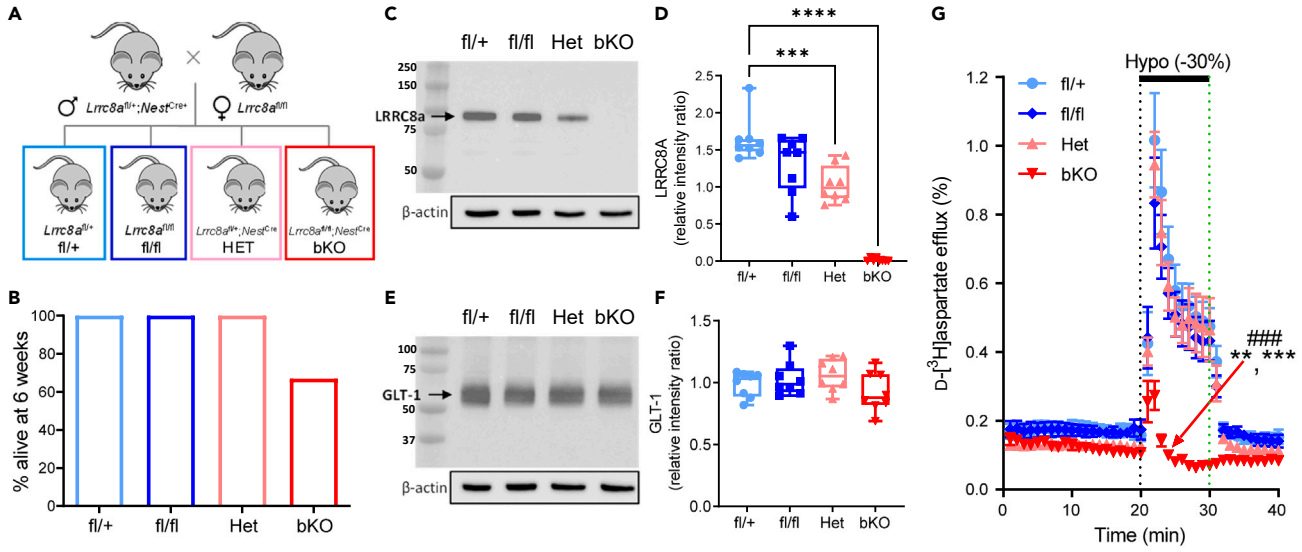

Figure 4. Validation of *Nestin*^{Cre} driven LRRC8A deletion *in vivo*

(A) Breeding strategy for the conditional deletion of LRRC8A in neurons, astrocytes, and oligodendrocytes using Nestin^{Cre}-strategy (bLRRC8A KO). The four potential genotypes from this breeding strategy are *Lrrc8a*$^{fl/+}$ (fl/+), *Lrrc8a*$^{fl/fl}$ (fl/fl), *Nestin*$^{Cre/+}$;*Lrrc8a*$^{fl/+}$ (Het), and *Nestin*$^{Cre/+}$;*Lrrc8a*$^{fl/fl}$ (bKO) mice.

(B) Survival rates among the four genotypes, with the bKO mice showing >30% mortality by the week six.

(C) Representative western blot image of LRRC8A expression in the whole brain lysates from four genotypes.

(D) Quantification of LRRC8A expression. The boxplot of individual IR values, normalized to β-actin loading and averaged within a set. n = 8/group. ***p<0.001, Het vs. fl/+, ****p<0.0001 bKO vs. fl/+. One way ANOVA with Tukey's multiple comparison test.

(E) Representative western blot image of GLT1 expression in the whole brain lysates from four genotypes.

(F) Quantification of GLT1 expression. The boxplot of individual IR values, normalized to β-actin loading and averaged within a set. n = 8/group.

(G) Assessment of swelling induced VRAC activity in primary astrocyte cultures, measured as D-[^{3}H]aspartate release in response to hypoosmotic medium superfusion. Data are the mean values ±SE of nine individual experiments per genotype from three different astrocyte cultures. **p <0.01, maximum release, KO versus fl/fl, ***p<0.001, KO vs. fl/+ and Het. $^{###}$p<0.001, integral (10-min) hypoosmotic release values, KO versus all other groups. Reproduced with permission from Wilson et al. (2021).

animals, GLT-1 levels were not statistically different between the four tested genotypes (Figures 4E and 4F; primary images in Figure S7). The discrepancy between the current and the prior work may be because of the younger age of animals analyzed in the current study.

VRAC activity is lost in bLRRC8A KO astrocytes but not affected by heterozygous bLRRC8A deletion

The functional loss of VRAC activity in bLRRC8A KO has been extensively characterized in our prior work[31] (reproduced with permission in Figure 4G. Copyright 2021 Federation of American Societies for Experimental Biology). The critical finding of this latter study is nearly complete loss of swelling-activated glutamate (D-[^{3}H]aspartate) release in bLRRC8A KO astrocytes (Figure 4G). The small residual D-[^{3}H]aspartate efflux present in the bKO cultures displays different time-dependent inactivation kinetics and may be mediated by a VRAC-independent release pathway(s). Equally important, astrocytic cultures derived from Het brains had virtually identical VRAC-mediated glutamate release as compared to fl/+ and fl/fl astrocyte controls (Figure 4G). This suggests that 20% and 40% reductions in LRRC8A protein levels in fl/fl and Het astrocytes, respectively, are insufficient to reduce plasmalemmal VRAC levels and activity. Taken together, these results confirmed the successful deletion of LRRC8A in bKO mice and the full functional VRAC activity in bLRRC8A Het animals.

Both complete and heterozygous bLRRC8A deletion reduces stroke damage

We independently reproduced the recent study by Zhou et al.[30] measuring stroke infarction volumes in bLRRC8A KO mice. One important addition in the present work was the use of four genotypes (fl/+, fl/fl, Het, and KO) rather than a straightforward comparison of WT to bLRRC8A KO animals in the aforementioned publication. As will be apparent from further discussion, the four-genotype comparison allowed for deeper interpretation of obtained results. Because of mortality in bLRRC8A KO mice, we

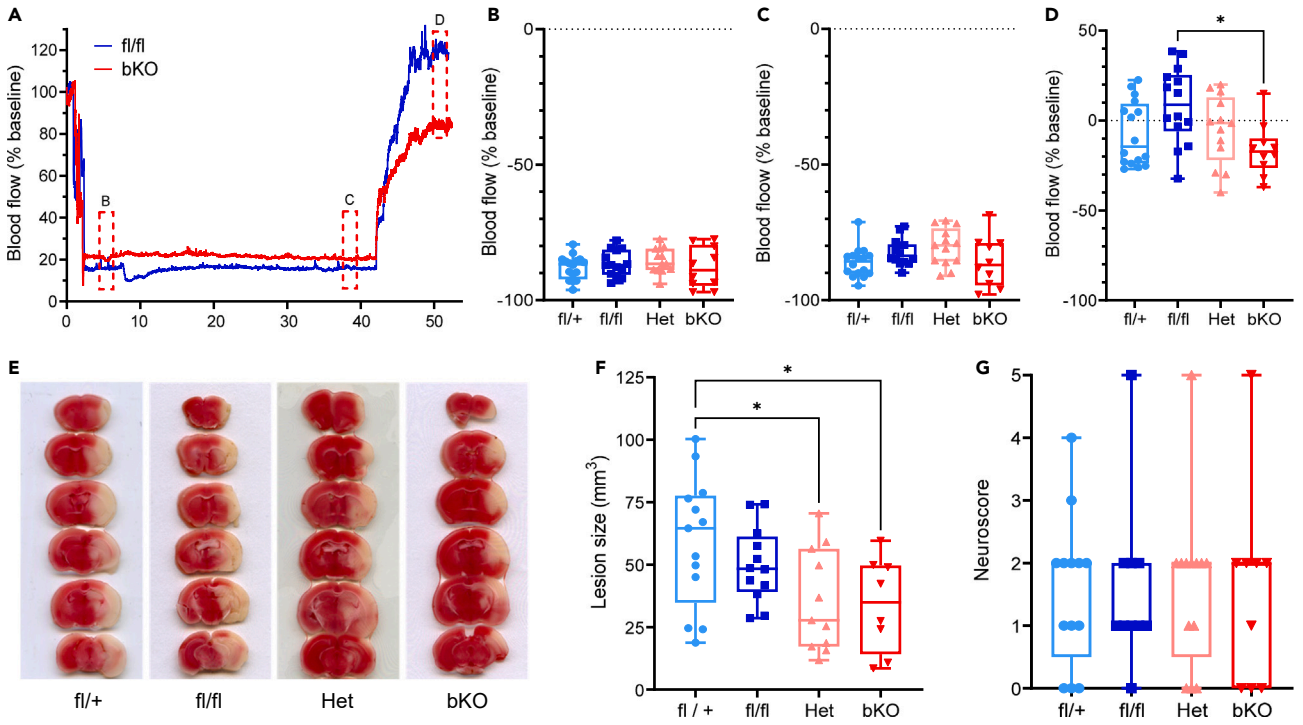

Figure 5. Effects of conditional brain-wide LRRC8A knockout (bLRRC8A KO) on primary and secondary outcomes in murine experimental stroke

(A) Representative changes in cerebral blood flow levels in bKO and control fl/fl mice during an MCAo experiment, measured using a laser Doppler flowmetry.

(B) The boxplot graph of the post-occlusion blood flow rates in mice from four genotype groups (indicated by 'B' in the representative graph). n = 10–16/group.

(C) The boxplot graph of the pre-reperfusion blood flow levels ('C'). n = 10–16/group.

(D) The boxplot graph of the blood flow recovery during initial reperfusion ('D'). n = 10–16/group. *p=0.016, fl/fl vs. bKO, one-way ANOVA with Tukey's correction for multiple comparisons.

(E) Representative TTC staining images of MCAo lesion volumes measured at 24 h poststroke.

(F) Boxplot graph and analysis of the primary outcome, the stroke infarction volumes corrected for brain edema, among four genotypes. *p<0.05, bKO vs. fl/+, Het vs. fl/+. One-way ANOVA with Tukey's correction for multiple comparisons. n = 8–13/group.

(G) Boxplot graph depicting quantitative comparison of neurological deficits in four genotypes measured at 24 h post-stroke as assessed by the five-point Neuroscore test.

used 6-6.5-week-old animals, which were subjected to a 40-min MCAo with reperfusion. To make our results directly comparable to the published work, we quantified stroke lesion volumes at 24 h rather than 72 h. Full animal use is reported in Figure S8.

For bLRRC8A KO experiments, we started with the comparisons of cerebral blood flow dynamics during and after MCAo (representative graphs in Figure 5A). As expected, we found a strong and persistent drop in blood flow during MCAo (Figure 5A). One way ANOVA found no differences among four genotypes immediately after occlusion and at the end of MCAo episode (Figures 5B and 5C). In the initial stages of reperfusion, blood flow values returned close to the pre-MCAo levels, with the exception of the bLRRC8A KO group showing ~20% blood flow deficit (representative chart and average values in Figures 5A–5D). It has been previously shown that glutamate release positively modulates blood flow via indirect effects on astrocytic production of eicosanoids.[46,47] This unexpected changes in cerebral blood flow prompted us to partially "relax" our pre-planned inclusion criterion for reperfusion. The post-hoc analysis indicated that the reperfusion deficit in bLRRC8A KO mice was statistically different from fl/fl group only (p = 0.012, Figure 5D). Overall, these data suggested that we have similar severity of ischemia in all genotypes, and that stroke outcomes in bLRRC8A KO group could be worsened by deficits in early reperfusion.

Our pre-planned primary outcome was the ischemic lesion size measured with a TTC approach. The 40-min MCAo produced large striatal and cortical infarction (representative images in Figure 5A), which highly

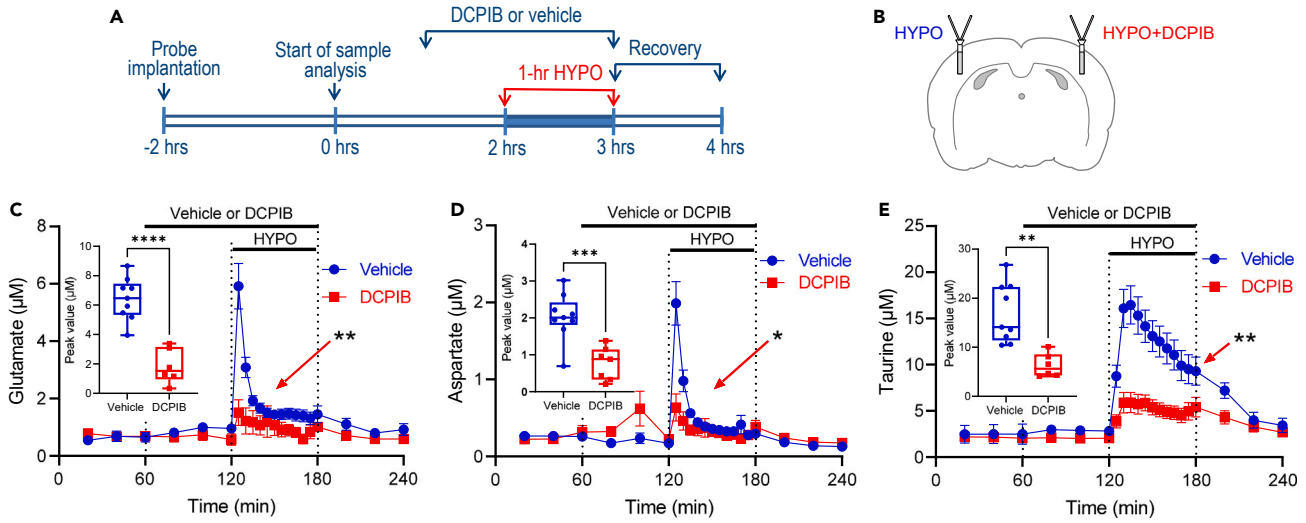

Figure 6. The effects of the VRAC blocker DCPIB on swelling-activated amino acid release *in vivo*

(A) Design of microdialysis experiments performed to test the efficacy of the VRAC inhibitor DCPIB *in vivo*.

(B) Schematic representation of microdialysis probe placements in the rat brain.

(C–E) The effect of hypoosmotic medium on the extracellular levels of glutamate (C), aspartate (D), and taurine (E) in microdialysis samples measured with an HPLC assay. In the C–E fields: *p<0.05, **p<0.01, DCPIB- versus vehicle-treated groups, the effects of treatment, time, and group-time interaction as analyzed with the mixed-effects model with Geisser-Greenhouse correction. Data are the mean values ±SE, n = 6–9/group. The box-plot insets show the peak values for individual amino acids during the hypoosmotic challenge. ***p<0.001, DCPIB versus Vehicle, t-test.

resembled the outcomes in older animals included in iaLRRC8A KO analysis (compare to Figure 3E). One way ANOVA of lesion sizes found that bLRRC8A KO and Het mice had significantly smaller brain infarctions as compared to the fl/+ group, with the reduction of 40+% (Figure 5F; all primary images in Figures S9 and S10). However, when the same two groups were compared against fl/fl controls, the statistical significance of neuroprotection was lost perhaps because of inherent variability of MCAo model (Figure 5F). One-way ANOVA comparisons of the secondary outcome, the neurological deficit on the five-point NeuroScore scale, did not reveal any differences among groups (Figure 5G). Overall, the results of stroke experiments in bLRRC8 KO mice and littermate controls showed a lack of correlation between infarction volumes and swelling-activated glutamate release.

Marginal effect of the VRAC blocker DCPIB on intraischemic glutamate release

To gain an additional insight into the mechanism of intraischemic glutamate release, we performed a microdialysis study quantifying extracellular levels of glutamate, aspartate, and taurine in stroke penumbra. The relatively large size of microdialysis probe (~2 mm length of semipermeable membrane cylinder) in relationship to small size of mouse brain does not allow for selective sampling of amino acids in penumbra. This is not a small matter because mechanisms of glutamate release fundamentally differ among ischemic regions. In the ischemic core, glutamate release is dominated by the reversal of glutamate transporters[17,48] whereas in the ischemic penumbra it is thought to be mediated by VRAC channels.[18,49] For this reason, we conducted microdialysis experiments in a rat model of stroke, as in our prior work.[50]

As a positive control for VRAC-mediated glutamate release, we tested the effect of DCPIB on glutamate levels in the rat cortex perfused with hypoosmotic artificial cerebrospinal fluid (aCSF). We and others validated this approach for measuring VRAC activity *in vivo* [*e.g.*,[51]]. As shown in Figure 6, perfusion of hypoosmotic solution triggered transient release of glutamate and two other VRAC-permeable amino acids, aspartate and taurine (Figures 6C–6E). When hypoosmotic medium was supplemented with the VRAC blocker DCPIB, stimulation of glutamate, aspartate and taurine release was inhibited by 71%, 74%, and 72% respectively (Figures 6C–6E). Altogether these experiments confirmed that cellular swelling dramatically upregulated release of VRAC-permeable amino acids, and that the chosen mode of DCPIB delivery is effective in limiting this process.

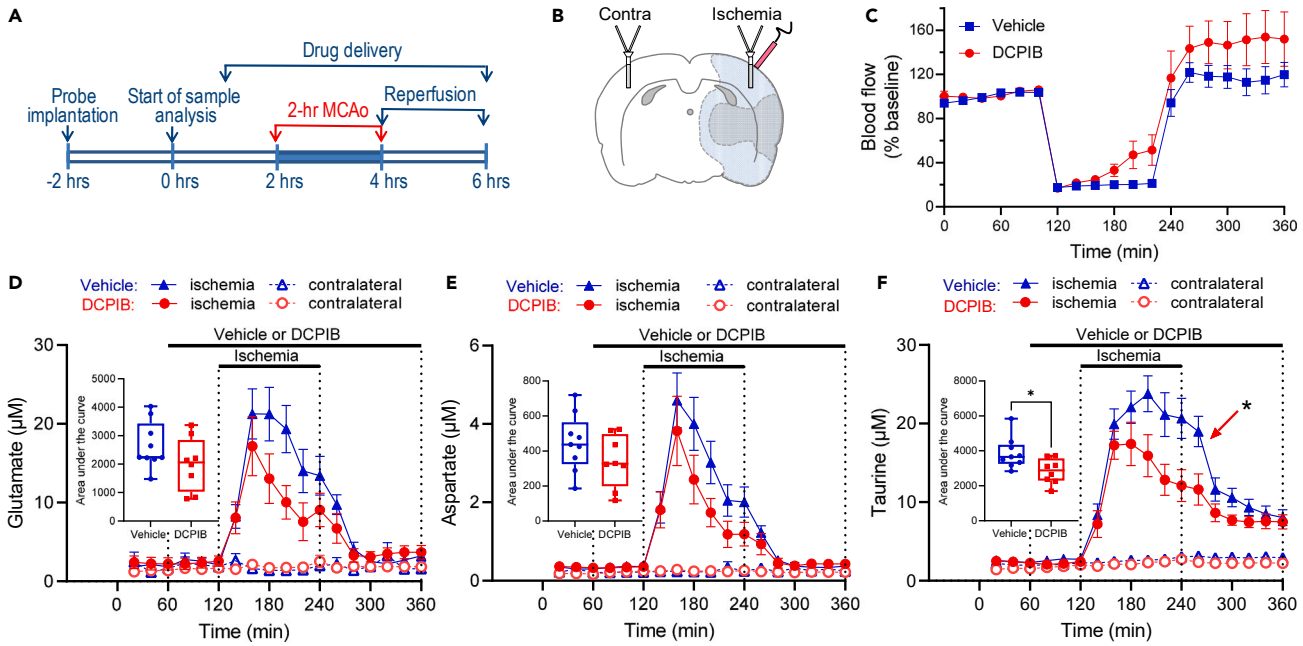

Figure 7. Marginal effects of the VRAC blocker DCPIB on the intraischemic amino acid release *in vivo*

(A) Design of microdialysis experiments performed to test the effects of the VRAC inhibitor DCPIB on pathological amino acid release in the rat MCAo stroke.

(B) Schematic representation of microdialysis and laser Doppler probe placements in the ischemic penumbra and corresponding contralateral location.

(C) The comparison of blood flow dynamics in Vehicle-and DCPIB-treated groups during and after MCAo, measured using a laser Doppler technique located as indicated in (B).

(D–F) The effect of DCPIB on the pathological extracellular levels of glutamate (D), aspartate (E), and taurine (F) in microdialysis samples collected during MCAo. In the F field: *p<0.05, DCPIB- vs. vehicle-treated taurine levels, the effects of treatment, time, and group-time interaction as analyzed with the mixed-effects model and Geisser-Greenhouse correction. Data are the mean values ±SE, n = 8–9/group. The box-plot insets show the integral release values for individual amino acids collected during the entire MCAo episode. *p<0.05, DCPIB versus Vehicle, t-test, reached significance for taurine only.

In the main set of experiments presented in Figure 7, microdialysis probes were placed in the same cortical areas as in hypoosmotic experiments, which now corresponded to ischemic penumbra or its anatomical equivalent in the contralateral hemisphere. The contralateral sampling was used to assure the long-term stability of microdialysis measurements and account for potential effects of probe-induced inflammation. The proper positioning of microdialysis probe in the penumbra was confirmed by a laser Doppler flowmetry as shown in Figure 7B. In both treatment groups, the initial reduction of cerebral perfusion was identical; however, the DCPIB-treated animals showed a trend for partial blood flow recovery during the middle cerebral artery occlusion period ($p = 0.094$ for group effect; $p = 0.208$ for group-time interaction; repeated measures ANOVA). Although this effect was not statistically significant, it might be relevant to changes in amino acid levels (see below). The 2-h occlusion of the MCA led to a dramatic increase in the extracellular levels of VRAC permeable glutamate (Figure 7D), aspartate (Figure 7E), and taurine (Figure 7F). Perfusion with DCPIB marginally reduced the intraischemic release of glutamate, aspartate, and taurine by 24, 24, and 26%, respectively (Figures 7D–7F, insets). Such a reduction reached the level of statistical significance for taurine only (Figure 7F). Overall, these results suggest small-to-negligible contribution of VRAC to the intraischemic amino acid release. Also, we cannot exclude that the effect of DCPIB was because of small improvements in the intraischemic blood flow (see Figure 7C) rather than direct inhibition of VRAC.

DISCUSSION

The major finding of our work is the disconnect between stroke outcomes and relative changes in VRAC activity in two mouse lines with targeted deletion of LRRC8A in brain cells (either in astrocytes only [iaLRRC8A KO] or neurons, astrocytes, and oligodendrocytes [the "brain-wide" bLRRC8A KO]). This surprising discovery is at odds with the widely accepted idea that multifunctional VRAC channels propagate tissue damage via pathological release of the excitatory neurotransmitters, glutamate and aspartate. The main argument against VRAC contributions to glutamate toxicity is the similar reduction of stroke infarction in

bLRRC8A KO mice carrying full LRRC8A deletion and their heterozygous littermates. Despite equal protection, bLRRC8A KO rodents have no functional VRAC in brain cells, whereas heterozygous mice exhibit full VRAC activity. These results strongly suggest that LRRC8A protein may promote ischemic brain damage via a mechanism(s) that is (are) unrelated to glutamate release.

Our first series of experiments tested the protective effect of inducible LRRC8A deletion in astrocytes (iaLRRC8A KO) using *Aldh1l1*^{CreERT2}. Astrocytes show the most prominent swelling in stroke and are thought to be the main source of pathological VRAC activity in the CNS.[13,52,53] Despite strong reductions in astroglial LRRC8A and VRAC-mediated glutamate release, we failed to detect predicted histological or behavioral protection in iaLRRC8A KO, as compared to three genotype/treatment controls. The lack of protection in our study differed from a ~30% reduction in the ischemic brain damage identified in a recent publication which used a non-inducible, *GFAP*^{Cre}-driven LRRC8A deletion in astrocytes.[29] The latter published gene deletion strategy targets astrocytes at early developmental stages and has small penetration to non-astrocytic cells.[54] Potential developmental compensation may be most relevant to discrepancies between two studies. In our hands, the *Nestin*^{Cre}-driven, brain-wide bLRRC8A excision, which occurs prenatally, causes substantial biochemical alterations in astrocytes and results in 100% animal mortality in early-to-late adolescence.[31] In contrast to bLRRC8A KO, the inducible iaLRRC8A KO in juvenile mice does not cause reactive astrogliosis or downregulation of astrocytic glutamate transporter GLT-1. The quantitative differences notwithstanding, the combined results of our work in iaLRRC8A KO and the study by Yang et al.[29] suggest that astrocytic LRRC8A/VRAC may contribute to but does not dominate ischemic brain damage.

The lack of neuroprotection in the iaLRRC8A KO is at odds with the prevalent concept that astrocytic VRAC is the key contributor in ischemic brain injury. This idea was introduced in the 1990s, based on the findings that hypoosmotic or high K^+-induced swelling of astrocytes opens an anion permeability pathway and triggers release of the excitotoxic glutamate and aspartate.[55,56] Because astroglia are known to be prominently swollen in stroke, it has been suggested that cell volume-sensitive glutamate release contributes to ischemic brain damage.[12,13,15] Accordingly, in rodent models of stroke, systemic delivery of the non-selective VRAC blocker tamoxifen decreased brain infarction volumes by as much as 60–80%.[19–22] The tamoxifen protection was seen in adult and neonatal rats, confirmed in both transient and permanent cerebral ischemia, and further corroborated in large animals, in the thromboembolic stroke model in dogs.[19–22,57] Together with subsequent reports of protection with a more selective VRAC inhibitor DCPIB,[49,58] these studies cemented the notion of VRAC as a promising target for stroke intervention. Yet, the major limitation of pharmacological studies is the numerous off-target effects of both tamoxifen and DCPIB. In the therapeutically relevant range of 1–10 μM, tamoxifen blocks diverse voltage-gated and ligand gated Na^+ and cation channels[59,60] or, alternatively, activates the BK subtype of K^+ channels.[61] It also inhibits neuronal and inducible isoforms of nitric oxide synthase and possesses significant antioxidant properties.[62,63] Likewise, the more specific DCPIB blocks several pathologically relevant glutamate release pathways and directly activates the BK K^+ channels and the two-pore domain K^+ channels.[64–66] On their own, these off-target effects could be neuroprotective, complicating interpretation of stroke findings. Thus, the exact mechanism for tamoxifen and DCPIB protection is not certain.

The caveats of pharmacological studies have been partially addressed by analyzing stroke outcomes in mice carrying conditional knockout of the essential VRAC subunit LRRC8A. The rather limited protection conveyed by astrocytic LRRC8A deletion seen in the prior publication[29] and the lack of protection in the current work are at odds with the potent reduction of ischemic damage by tamoxifen and DCPIB. Of interest, another publication found more robust (~50%) reduction of stroke damage in mice carrying the brain-wide LRRC8A knockout produced with *Nestin*^{Cre}.[30] Perhaps, these latter results suggest that under pathological conditions, VRAC is active in numerous brain cell types. To definitively examine this idea, we re-evaluated stroke outcomes in the *Nestin*^{Cre}-driven, brain-wide LRRC8A KO mice. bLRRC8A KO animals show the complete loss of brain LRRC8A immunoreactivity, electrophysiological VRAC currents, and swelling-activated glutamate release.[29–31] Using this genetic strategy, Zhou and coworkers compared cerebral infarction in the two genotypes, *Lrrc8a*$^{fl/fl}$ controls and LRRC8A KO.[30] For additional rigor, we tested stroke outcomes in four distinct genotypes (two controls, *Lrrc8a*$^{fl/+}$ and *Lrrc8a*$^{fl/fl}$, heterozygous b*Lrrc8a* deletion, and full b*Lrrc8a* KO). Such extended analysis proved to be critical. Consistent with the prior publication, we found that the bLRRC8A KO brains were strongly protected against stroke as compared to fl/+ littermates, with the reduction in infarction volumes reaching 40+%. Yet, when bLRRC8A KO results were

analyzed against fl/fl controls, the average protection was smaller and not statistically significant. However, the key finding came from the assessment of bLRRC8A Het mice. *LRRC8A KO and Het animals were equally protected against stroke, even though LRRC8A Het cells retained full VRAC activity*. In our judgment, a complete disconnect between VRAC activity and stroke outcomes rules out a significant role for the VRAC-mediated glutamate release in acute ischemic stroke injury.

To additionally probe the pathological contributions of VRAC we employed a microdialysis approach and measured glutamate levels in the ischemic penumbra. Because of the smaller size of the mouse brain, these experiments were conducted in rats. As with several prior studies, we found dramatic elevation in the extracellular levels of glutamate and the other VRAC permeable neurotransmitters, aspartate and taurine. Yet, in our hands, the VRAC blocker DCPIB showed minor impact on pathological amino acid release. Together with the lack of correlation between swelling-activated glutamate release and neuroprotection in our genetically modified animals, these results support the conclusion that VRAC-mediated glutamate release does not dominate excitotoxic tissue damage in the ischemic penumbra. The apparent lack of VRAC activity in stroke tissue may be explained by the requirement of non-hydrolytic ATP binding for VRAC channel opening.[6–8] Metabolic inhibition or omission of ATP from pipette solution eliminates swelling-activated Cl^- currents and amino acid release.[67–70] This high dependence on cytosolic ATP or other nucleotide triphosphates is likely to limit VRAC activity in metabolically compromised ischemic tissue, particularly in non-astroglial cells, and explains our microdialysis results.

If swelling-activated glutamate release is not involved, then why are LRRC8A Het and KO brains protected against stroke? One speculation is that changes in LRRC8A protein expression may modify pro-death intracellular machinery in neural cells. Besides its essential role in the VRAC channel activity,[23,24] LRRC8A protein additionally serves as a signaling scaffold molecule. Thus, LRRC8A physically interacts with two important adaptor molecules, Growth factor Receptor-Bound protein 2 (GRB2) and GRB2-Associated Binding protein 2 (GAB2), and in such a way potently modulates downstream signaling cascades and modifies many cellular functions.[71–74] Among the relevant pathways, LRRC8A expression seems to regulate activities of c-Jun N-terminal kinases (JNK).[75,76] JNK isoforms, and particularly JNK3 promote ischemic/hypoxic brain injury and their acute inhibition protects against stroke damage in mice.[77–80] We speculate that reductions in LRRC8A levels seen in Het and bLRRC8A KO animals could modulate this or another intracellular signaling cascade and reduce stroke damage. However, such a hypothesis requires further exploration.

The practical implication of our work is that the utility of *selective* inhibition of VRAC for reducing ischemic brain damage needs to be re-evaluated. Over the years, the field accumulated strong evidence for neuroprotective actions of the putative VRAC blockers, tamoxifen and DCPIB. Yet, based on our findings the protection by these agents appears to be largely unrelated to the VRAC-mediated glutamate release. Likewise, stroke protection in mice with targeted deletion of the essential VRAC subunit LRRC8A, may also be weakly related to glutamate toxicity and engage distinct molecular processes. From a broader prospective, the present study reinforces the idea that the LRRC8A deletion experiments need to be interpreted while both considering modification of VRAC channel function but also channel-unrelated mechanisms.

Limitations of the study

Although our work has comprehensively tested pathological significance of swelling-activated glutamate release in stroke, it is not without caveats. The main limitation is that, because of technical constraints, we were not able to measure intraischemic glutamate levels in the genetically modified mice. The mouse brain is too small for microdialysis sampling in the ischemic penumbra. Therefore, as a proxy we used microdialysis in conjunction with a pharmacological VRAC blocker in rats. Although the rat data are consistent with findings in a mouse, potential interspecies differences should be kept in mind. The second limitation is that the inducible deletion of LRRC8A in mouse astrocytes affected the majority but not all targeted cells (98% of cre-positive astrocytes in hippocampus, but 90% in the cortical tissue). This may be relevant to the differences in brain protection in our study and the work by Yang et al.,[29] which generated a non-inducible astrocytic LRRC8A knockout. These two limitations do not impact the major conclusion of the present investigation. Finally, at this stage we are yet to pinpoint the precise mechanisms for brain protection in mice carrying the "brain-wide" heterozygous and homozygous LRRC8A deletion. It was beyond the scope of the current study. Addressing the latter question represents an opportunity for the field to uncover new mechanisms of ischemic brain damage and stroke resilience.

STAR★METHODS

Detailed methods are provided in the online version of this paper and include the following:

- KEY RESOURCES TABLE
- RESOURCE AVAILABILITY
  - Lead contact
  - Materials availability
  - Data and code availability
- EXPERIMENTAL MODEL AND SUBJECT DETAILS
  - Ethics statement
  - Animals
- METHOD DETAILS
  - Cell cultures of brain astrocytes
  - Processing of brain tissue samples
  - Immunohistochemistry
  - Western blotting analysis
  - VRAC activity assay
  - Middle cerebral artery occlusion surgery in mice
  - Brain lesion measurements
  - Evaluation of neurological deficits
  - Middle cerebral artery occlusion surgery and microdialysis in rats
  - Analysis of microdialysate samples
- QUANTIFICATION AND STATISTICAL ANALYSIS

SUPPLEMENTAL INFORMATION

Supplemental information can be found online at https://doi.org/10.1016/j.isci.2023.106669.

ACKNOWLEDGMENTS

This work was supported by NIH/NINDS grant R01 NS111943 (to A.A.M.). The Authors thank Dr. Aarshi Vipani for contributions to processing rat microdialysis experiments and Dr. Paul J. Feustel for help and advice. The graphical summary was prepared using Motfolio scientific illustration toolkits (motfolio.com).

AUTHOR CONTRIBUTIONS

Conceptualization: A.A.M.; Methodology: M.B., P.D., A.L.S., and A.A.M.; Investigation: M.B, P.D., S.C., A.L.S., A.M.F., and J.W.N; Writing – Original Draft: M.B and A.A.M.; Writing – Review and Editing: A.A.M, M.B., P.D., S.C., A.L.S., A.M.F., J.W.N., and R.S.; Unique Resources: R.S.; Funding Acquisition: A.A.M.; Supervision: A.A.M.

DECLARATION OF INTERESTS

One of the co-authors of this manuscript (R.S.) has pending patent applications covering the use of LRRC8 complex modulators for therapeutic purposes. Other authors declare no competing interests.

Received: December 30, 2022
Revised: March 3, 2023
Accepted: April 11, 2023
Published: April 14, 2023

REFERENCES

1. Sacco, R.L., Kasner, S.E., Broderick, J.P., Caplan, L.R., Connors, J.J.B., Culebras, A., Elkind, M.S.V., George, M.G., Hamdan, A.D., Higashida, R.T., et al.; American Heart Association Stroke Council, Council on Cardiovascular Surgery and Anesthesia; Council on Cardiovascular Radiology and Intervention; Council on Cardiovascular and Stroke Nursing; Council on Epidemiology and Prevention; Council on Peripheral Vascular Disease; Council on Nutrition, Physical Activity and Metabolism (2013). An updated definition of stroke for the 21st century: a statement for healthcare professionals from the American Heart Association/American Stroke Association. Stroke 44, 2064–2089.

2. Campbell, B.C.V., De Silva, D.A., Macleod, M.R., Coutts, S.B., Schwamm, L.H., Davis, S.M., and Donnan, G.A. (2019). Ischaemic stroke. Nat. Rev. Dis. Prim. 5, 70.

3. Feigin, V.L., Brainin, M., Norrving, B., Martins, S., Sacco, R.L., Hacke, W., Fisher, M., Pandian, J., and Lindsay, P. (2022). World stroke organization (WSO): global

stroke fact sheet 2022. Int. J. Stroke *17*, 18–29.

4. Ginsberg, M.D. (2008). Neuroprotection for ischemic stroke: past, present and future. Neuropharmacology *55*, 363–389.

5. Paul, S., and Candelario-Jalil, E. (2021). Emerging neuroprotective strategies for the treatment of ischemic stroke: an overview of clinical and preclinical studies. Exp. Neurol. *335*, 113518.

6. Strange, K., Emma, F., and Jackson, P.S. (1996). Cellular and molecular physiology of volume-sensitive anion channels. Am. J. Physiol. *270*, C711–C730.

7. Okada, Y. (1997). Volume expansion-sensing outward-rectifier Cl- channel: fresh start to the molecular identity and volume sensor. Am. J. Physiol. *273*, C755–C789.

8. Nilius, B., Eggermont, J., Voets, T., Buyse, G., Manolopoulos, V., and Droogmans, G. (1997). Properties of volume-regulated anion channels in mammalian cells. Prog. Biophys. Mol. Biol. *68*, 69–119.

9. Hoffmann, E.K., Lambert, I.H., and Pedersen, S.F. (2009). Physiology of cell volume regulation in vertebrates. Physiol. Rev. *89*, 193–277.

10. Pedersen, S.F., Okada, Y., and Nilius, B. (2016). Biophysics and physiology of the volume-regulated anion channel (VRAC)/volume-sensitive outwardly rectifying anion channel (VSOR). Pflügers Archiv *468*, 371–383.

11. Jentsch, T.J. (2016). VRACs and other ion channels and transporters in the regulation of cell volume and beyond. Nat. Rev. Mol. Cell Biol. *17*, 293–307.

12. Kimelberg, H.K., and Mongin, A.A. (1998). Swelling-activated release of excitatory amino acids in the brain: relevance for pathophysiology. Contrib. Nephrol. *123*, 240–257.

13. Kimelberg, H.K. (2005). Astrocytic swelling in cerebral ischemia as a possible cause of injury and target for therapy. Glia *50*, 389–397.

14. Mongin, A.A. (2016). Volume-regulated anion channel–a frenemy within the brain. Pflügers Archiv *468*, 421–441.

15. Mongin, A.A. (2007). Disruption of ionic and cell volume homeostasis in cerebral ischemia: the perfect storm. Pathophysiology *14*, 183–193.

16. Phillis, J.W., Song, D., and O'Regan, M.H. (1998). Tamoxifen, a chloride channel blocker, reduces glutamate and aspartate release from the ischemic cerebral cortex. Brain Res. *780*, 352–355.

17. Seki, Y., Feustel, P.J., Keller, R.W., Jr., Tranmer, B.I., and Kimelberg, H.K. (1999). Inhibition of ischemia-induced glutamate release in rat striatum by dihydrokinate and an anion channel blocker. Stroke *30*, 433–440.

18. Feustel, P.J., Jin, Y., and Kimelberg, H.K. (2004). Volume-regulated anion channels are the predominant contributors to release of excitatory amino acids in the ischemic cortical penumbra. Stroke *35*, 1164–1168.

19. Kimelberg, H.K., Feustel, P.J., Jin, Y., Paquette, J., Boulos, A., Keller, R.W., Jr., and Tranmer, B.I. (2000). Acute treatment with tamoxifen reduces ischemic damage following middle cerebral artery occlusion. Neuroreport *11*, 2675–2679.

20. Kimelberg, H.K., Jin, Y., Charniga, C., and Feustel, P.J. (2003). Neuroprotective activity of tamoxifen in permanent focal ischemia. J. Neurosurg. *99*, 138–142.

21. Mehta, S.H., Dhandapani, K.M., De Sevilla, L.M., Webb, R.C., Mahesh, V.B., and Brann, D.W. (2003). Tamoxifen, a selective estrogen receptor modulator, reduces ischemic damage caused by middle cerebral artery occlusion in the ovariectomized female rat. Neuroendocrinology *77*, 44–50.

22. Feng, Y., Fratkins, J.D., and LeBlanc, M.H. (2004). Treatment with tamoxifen reduces hypoxic-ischemic brain injury in neonatal rats. Eur. J. Pharmacol. *484*, 65–74.

23. Qiu, Z., Dubin, A.E., Mathur, J., Tu, B., Reddy, K., Miraglia, L.J., Reinhardt, J., Orth, A.P., and Patapoutian, A. (2014). SWELL1, a plasma membrane protein, is an essential component of volume-regulated anion channel. Cell *157*, 447–458.

24. Voss, F.K., Ullrich, F., Münch, J., Lazarow, K., Lutter, D., Mah, N., Andrade-Navarro, M.A., von Kries, J.P., Stauber, T., and Jentsch, T.J. (2014). Identification of LRRC8 heteromers as an essential component of the volume-regulated anion channel VRAC. Science *344*, 634–638.

25. Deneka, D., Sawicka, M., Lam, A.K.M., Paulino, C., and Dutzler, R. (2018). Structure of a volume-regulated anion channel of the LRRC8 family. Nature *558*, 254–259.

26. Kasuya, G., Nakane, T., Yokoyama, T., Jia, Y., Inoue, M., Watanabe, K., Nakamura, R., Nishizawa, T., Kusakizako, T., Tsutsumi, A., et al. (2018). Cryo-EM structures of the human volume-regulated anion channel LRRC8. Nat. Struct. Mol. Biol. *25*, 797–804.

27. Kefauver, J.M., Saotome, K., Dubin, A.E., Pallesen, J., Cottrell, C.A., Cahalan, S.M., Qiu, Z., Hong, G., Crowley, C.S., Whitwam, T., et al. (2018). Structure of the human volume regulated anion channel. Elife *7*, e38461.

28. Nakamura, R., Numata, T., Kasuya, G., Yokoyama, T., Nishizawa, T., Kusakizako, T., Kato, T., Hagino, T., Dohmae, N., Inoue, M., et al. (2020). Cryo-EM structure of the volume-regulated anion channel LRRC8D isoform identifies features important for substrate permeation. Commun. Biol. *3*, 240.

29. Yang, J., Vitery, M.D.C., Chen, J., Osei-Owusu, J., Chu, J., and Qiu, Z. (2019). Glutamate-releasing SWELL1 channel in astrocytes modulates synaptic transmission and promotes brain damage in stroke. Neuron *102*, 813–827.e6.

30. Zhou, J.J., Luo, Y., Chen, S.R., Shao, J.Y., Sah, R., and Pan, H.L. (2020). LRRC8A-dependent volume-regulated anion channels contribute to ischemia-induced brain injury and glutamatergic input to hippocampal neurons. Exp. Neurol. *332*, 113391.

31. Wilson, C.S., Dohare, P., Orbeta, S., Nalwalk, J.W., Huang, Y., Ferland, R.J., Sah, R., Scimemi, A., and Mongin, A.A. (2021). Late adolescence mortality in mice with brain-specific deletion of the volume-regulated anion channel subunit LRRC8A. Faseb. J. *35*, e21869.

32. Srinivasan, R., Lu, T.Y., Chai, H., Xu, J., Huang, B.S., Golshani, P., Coppola, G., and Khakh, B.S. (2016). New transgenic mouse lines for selectively targeting astrocytes and studying calcium signals in astrocyte processes in situ and in vivo. Neuron *92*, 1181–1195.

33. Cahoy, J.D., Emery, B., Kaushal, A., Foo, L.C., Zamanian, J.L., Christopherson, K.S., Xing, Y., Lubischer, J.L., Krieg, P.A., Krupenko, S.A., et al. (2008). A transcriptome database for astrocytes, neurons, and oligodendrocytes: a new resource for understanding brain development and function. J. Neurosci. *28*, 264–278.

34. Jahn, H.M., Kasakow, C.V., Helfer, A., Michely, J., Verkhratsky, A., Maurer, H.H., Scheller, A., and Kirchhoff, F. (2018). Refined protocols of tamoxifen injection for inducible DNA recombination in mouse astroglia. Sci. Rep. *8*, 5913.

35. Khakh, B.S., and Sofroniew, M.V. (2015). Diversity of astrocyte functions and phenotypes in neural circuits. Nat. Neurosci. *18*, 942–952.

36. Abdullaev, I.F., Rudkouskaya, A., Schools, G.P., Kimelberg, H.K., and Mongin, A.A. (2006). Pharmacological comparison of swelling-activated excitatory amino acid release and Cl- currents in rat cultured astrocytes. J. Physiol. *572*, 677–689.

37. Hyzinski-García, M.C., Rudkouskaya, A., and Mongin, A.A. (2014). LRRC8A protein is indispensable for swelling-activated and ATP-induced release of excitatory amino acids in rat astrocytes. J. Physiol. *592*, 4855–4862.

38. Hossmann, K.A. (1994). Viability thresholds and the penumbra of focal ischemia. Ann. Neurol. *36*, 557–565.

39. Belayev, L., Busto, R., Zhao, W., Fernandez, G., and Ginsberg, M.D. (1999). Middle cerebral artery occlusion in the mouse by intraluminal suture coated with poly-L-lysine: neurological and histological validation. Brain Res. *833*, 181–190.

40. Balkaya, M., Kim, I.D., Shakil, F., and Cho, S. (2021). CD36 deficiency reduces chronic BBB dysfunction and scar formation and improves activity, hedonic and memory deficits in ischemic stroke. J. Cerebr. Blood Flow Metabol. *41*, 486–501.

41. Balkaya, M., Kröber, J.M., Rex, A., and Endres, M. (2013). Assessing post-stroke behavior in mouse models of focal ischemia. J. Cerebr. Blood Flow Metabol. *33*, 330–338.

42. Dubois, N.C., Hofmann, D., Kaloulis, K., Bishop, J.M., and Trumpp, A. (2006). Nestin-Cre transgenic mouse line Nes-Cre1 mediates highly efficient Cre/loxP mediated recombination in the nervous system, kidney, and somite-derived tissues. Genesis *44*, 355–360.

43. Lagace, D.C., Whitman, M.C., Noonan, M.A., Ables, J.L., DeCarolis, N.A., Arguello, A.A., Donovan, M.H., Fischer, S.J., Farnbauch, L.A., Beech, R.D., et al. (2007). Dynamic contribution of nestin-expressing stem cells to adult neurogenesis. J. Neurosci. *27*, 12623–12629.

44. Rao, V.L., Dogan, A., Todd, K.G., Bowen, K.K., Kim, B.T., Rothstein, J.D., and Dempsey, R.J. (2001). Antisense knockdown of the glial glutamate transporter GLT-1, but not the neuronal glutamate transporter EAAC1, exacerbates transient focal cerebral ischemia-induced neuronal damage in rat brain. J. Neurosci. *21*, 1876–1883.

45. Harvey, B.K., Airavaara, M., Hinzman, J., Wires, E.M., Chiocco, M.J., Howard, D.B., Shen, H., Gerhardt, G., Hoffer, B.J., and Wang, Y. (2011). Targeted over-expression of glutamate transporter 1 (GLT-1) reduces ischemic brain injury in a rat model of stroke. PLoS One *6*, e22135.

46. Alkayed, N.J., Birks, E.K., Narayanan, J., Petrie, K.A., Kohler-Cabot, A.E., and Harder, D.R. (1997). Role of P-450 arachidonic acid epoxygenase in the response of cerebral blood flow to glutamate in rats. Stroke *28*, 1066–1072.

47. Zonta, M., Angulo, M.C., Gobbo, S., Rosengarten, B., Hossmann, K.A., Pozzan, T., and Carmignoto, G. (2003). Neuron-to-astrocyte signaling is central to the dynamic control of brain microcirculation. Nat. Neurosci. *6*, 43–50.

48. Phillis, J.W., Smith-Barbour, M., Perkins, L.M., and O'Regan, M.H. (1994). Characterization of glutamate, aspartate, and GABA release from ischemic rat cerebral cortex. Brain Res. Bull. *34*, 457–466.

49. Zhang, Y., Zhang, H., Feustel, P.J., and Kimelberg, H.K. (2008). DCPIB, a specific inhibitor of volume regulated anion channels (VRACs), reduces infarct size in MCAo and the release of glutamate in the ischemic cortical penumbra. Exp. Neurol. *210*, 514–520.

50. Dohare, P., Hyzinski-García, M.C., Vipani, A., Bowens, N.H., Nalwalk, J.W., Feustel, P.J., Keller, R.W., Jr., Jourd'heuil, D., and Mongin, A.A. (2014). The neuroprotective properties of the superoxide dismutase mimetic tempol correlate with its ability to reduce pathological glutamate release in a rodent model of stroke. Free Radic. Biol. Med. *77*, 168–182.

51. Haskew-Layton, R.E., Rudkouskaya, A., Jin, Y., Feustel, P.J., Kimelberg, H.K., and Mongin, A.A. (2008). Two distinct modes of hypoosmotic medium-induced release of excitatory amino acids and taurine in the rat brain in vivo. PLoS One *3*, e3543.

52. Mongin, A.A., and Kimelberg, H.K. (2005). Astrocytic swelling in neuropathology. In Neuroglia, 2nd ed., H. Kettenmann and B.R. Ransom, eds. (Oxford University Press), pp. 550–562.

53. Wilson, C.S., and Mongin, A.A. (2018). Cell volume control in healthy brain and neuropathologies. Curr. Top. Membr. *81*, 385–455.

54. Sofroniew, M.V. (2012). Transgenic techniques for cell ablation or molecular deletion to investigate functions of astrocytes and other GFAP-expressing cell types. Methods Mol. Biol. *814*, 531–544.

55. Kimelberg, H.K., Goderie, S.K., Higman, S., Pang, S., and Waniewski, R.A. (1990). Swelling-induced release of glutamate, aspartate, and taurine from astrocyte cultures. J. Neurosci. *10*, 1583–1591.

56. Rutledge, E.M., and Kimelberg, H.K. (1996). Release of [3H]-D-aspartate from primary astrocyte cultures in response to raised external potassium. J. Neurosci. *16*, 7803–7811.

57. Boulos, A.S., Deshaies, E.M., Dalfino, J.C., Feustel, P.J., Popp, A.J., and Drazin, D. (2011). Tamoxifen as an effective neuroprotectant in an endovascular canine model of stroke. J. Neurosurg. *114*, 1117–1126.

58. Alibrahim, A., Zhao, L.Y., Bae, C.Y.j., Barszczyk, A., Sun, C.L.F., Wang, G.L., and Sun, H.S. (2013). Neuroprotective effects of volume-regulated anion channel blocker DCPIB on neonatal hypoxic-ischemic injury. Acta Pharmacol. Sin. *34*, 113–118.

59. Allen, M.C., Newland, C., Valverde, M.A., and Hardy, S.P. (1998). Inhibition of ligand-gated cation-selective channels by tamoxifen. Eur. J. Pharmacol. *354*, 261–269.

60. Hardy, S.P., deFelipe, C., and Valverde, M.A. (1998). Inhibition of voltage-gated cationic channels in rat embryonic hypothalamic neurones and C1300 neuroblastoma cells by triphenylethylene antioestrogens. FEBS Lett. *434*, 236–240.

61. He, J., Kargacin, M.E., Kargacin, G.J., and Ward, C.A. (2003). Tamoxifen inhibits Na^+ and K^+ currents in rat ventricular myocytes. Am. J. Physiol. Heart Circ. Physiol. *285*, H661–H668.

62. Osuka, K., Feustel, P.J., Mongin, A.A., Tranmer, B.I., and Kimelberg, H.K. (2001). Tamoxifen inhibits nitrotyrosine formation after reversible middle cerebral artery occlusion in the rat. J. Neurochem. *76*, 1842–1850.

63. Custódio, J.B., Dinis, T.C., Almeida, L.M., and Madeira, V.M. (1994). Tamoxifen and hydroxytamoxifen as intramembraneous inhibitors of lipid peroxidation. Evidence for peroxyl radical scavenging activity. Biochem. Pharmacol. *47*, 1989–1998.

64. Bowens, N.H., Dohare, P., Kuo, Y.H., and Mongin, A.A. (2013). DCPIB, the proposed selective blocker of volume-regulated anion channels, inhibits several glutamate transport pathways in glial cells. Mol. Pharmacol. *83*, 22–32.

65. Minieri, L., Pivonkova, H., Caprini, M., Harantova, L., Anderova, M., and Ferroni, S. (2013). The inhibitor of volume-regulated anion channels DCPIB activates TREK potassium channels in cultured astrocytes. Br. J. Pharmacol. *168*, 1240–1254.

66. Zuccolini, P., Ferrera, L., Remigante, A., Picco, C., Barbieri, R., Bertelli, S., Moran, O., Gavazzo, P., and Pusch, M. (2022). The VRAC blocker DCPIB directly gates the BK channels and increases intracellular Ca(2+) in melanoma and pancreatic duct adenocarcinoma cell lines. Br. J. Pharmacol. *179*, 3452–3469.

67. Jackson, P.S., Morrison, R., and Strange, K. (1994). The volume-sensitive organic osmolyte-anion channel VSOAC is regulated by nonhydrolytic ATP binding. Am. J. Physiol. *267*, C1203–C1209.

68. Oike, M., Droogmans, G., and Nilius, B. (1994). The volume-activated chloride current in human endothelial cells depends on intracellular ATP. Pflügers Archiv *427*, 184–186.

69. Oiki, S., Kubo, M., and Okada, Y. (1994). Mg2+ and ATP-dependence of volume-sensitive Cl- channels in human epithelial cells. Jpn. J. Physiol. *44* (*Suppl 2*), S77–S79.

70. Rutledge, E.M., Mongin, A.A., and Kimelberg, H.K. (1999). Intracellular ATP depletion inhibits swelling-induced D-[^{3}H] aspartate release from primary astrocyte cultures. Brain Res. *842*, 39–45.

71. Kumar, L., Chou, J., Yee, C.S.K., Borzutzky, A., Vollmann, E.H., von Andrian, U.H., Park, S.Y., Hollander, G., Manis, J.P., Poliani, P.L., and Geha, R.S. (2014). Leucine-rich repeat containing 8A (LRRC8A) is essential for T lymphocyte development and function. J. Exp. Med. *211*, 929–942.

72. Zhang, Y., Xie, L., Gunasekar, S.K., Tong, D., Mishra, A., Gibson, W.J., Wang, C., Fidler, T., Marthaler, B., Klingelhutz, A., et al. (2017). SWELL1 is a regulator of adipocyte size, insulin signalling and glucose homeostasis. Nat. Cell Biol. *19*, 504–517.

73. Kumar, A., Xie, L., Ta, C.M., Hinton, A.O., Gunasekar, S.K., Minerath, R.A., Shen, K., Maurer, J.M., Grueter, C.E., Abel, E.D., et al. (2020). SWELL1 regulates skeletal muscle cell size, intracellular signaling, adiposity and glucose metabolism. Elife *9*, e58941.

74. Alghanem, A.F., Abello, J., Maurer, J.M., Kumar, A., Ta, C.M., Gunasekar, S.K., Fatima, U., Kang, C., Xie, L., Adeola, O., et al. (2021). The SWELL1-LRRC8 complex regulates endothelial AKT-eNOS signaling and vascular function. Elife *10*, e61313.

75. Choi, H., Ettinger, N., Rohrbough, J., Dikalova, A., Nguyen, H.N., and Lamb, F.S. (2016). LRRC8A channels support TNFalpha-induced superoxide production by Nox1

which is required for receptor endocytosis. Free Radic. Biol. Med. *101*, 413–423.

76. Lu, P., Ding, Q., Li, X., Ji, X., Li, L., Fan, Y., Xia, Y., Tian, D., and Liu, M. (2019). SWELL1 promotes cell growth and metastasis of hepatocellular carcinoma in vitro and in vivo. EBioMedicine *48*, 100–116.

77. Kuan, C.Y., Whitmarsh, A.J., Yang, D.D., Liao, G., Schloemer, A.J., Dong, C., Bao, J., Banasiak, K.J., Haddad, G.G., Flavell, R.A., et al. (2003). A critical role of neural-specific JNK3 for ischemic apoptosis. Proc. Natl. Acad. Sci. USA *100*, 15184–15189.

78. Borsello, T., Clarke, P.G.H., Hirt, L., Vercelli, A., Repici, M., Schorderet, D.F., Bogousslavsky, J., and Bonny, C. (2003). A peptide inhibitor of c-Jun N-terminal kinase protects against excitotoxicity and cerebral ischemia. Nat. Med. *9*, 1180–1186.

79. Gao, Y., Signore, A.P., Yin, W., Cao, G., Yin, X.M., Sun, F., Luo, Y., Graham, S.H., and Chen, J. (2005). Neuroprotection against focal ischemic brain injury by inhibition of c-Jun N-terminal kinase and attenuation of the mitochondrial apoptosis-signaling pathway. J. Cerebr. Blood Flow Metabol. *25*, 694–712.

80. Pirianov, G., Brywe, K.G., Mallard, C., Edwards, A.D., Flavell, R.A., Hagberg, H., and Mehmet, H. (2007). Deletion of the c-Jun N-terminal kinase 3 gene protects neonatal mice against cerebral hypoxic-ischaemic injury. J. Cereb. Blood Flow Metab. *27*, 1022–1032.

81. Schober, A.L., Wilson, C.S., and Mongin, A.A. (2017). Molecular composition and heterogeneity of the LRRC8-containing swelling-activated osmolyte channels in primary rat astrocytes. J. Physiol. *595*, 6939–6951.

82. Bederson, J.B., Pitts, L.H., Germano, S.M., Nishimura, M.C., Davis, R.L., and Bartkowski, H.M. (1986). Evaluation of 2,3,5-triphenyltetrazolium chloride as a stain for detection and quantification of experimental cerebral infarction in rats. Stroke *17*, 1304–1308.

83. Rasband, W.S. (1997). ImageJ. http://imagej.nih.gov/ij.

84. Swanson, R.A., Morton, M.T., Tsao-Wu, G., Savalos, R.A., Davidson, C., and Sharp, F.R. (1990). A semiautomated method for measuring brain infarct volume. J. Cerebr. Blood Flow Metabol. *10*, 290–293.

85. Balkaya, M.G., Trueman, R.C., Boltze, J., Corbett, D., and Jolkkonen, J. (2018). Behavioral outcome measures to improve experimental stroke research. Behav. Brain Res. *352*, 161–171.

86. Longa, E.Z., Weinstein, P.R., Carlson, S., and Cummins, R. (1989). Reversible middle cerebral artery occlusion without craniectomy in rats. Stroke *20*, 84–91.

STAR★METHODS

KEY RESOURCES TABLE

REAGENT or RESOURCE	SOURCE	IDENTIFIER
Antibodies		
Mouse monoclonal anti-β-actin antibody, HRP-conjugated	Millipore-Sigma	cat. #A3854; RRID:AB_262011
Rabbit polyclonal anti-GLT1 (EAAT2)	Abcam	cat. #ab41621; RRID:AB_941782
Mouse monoclonal anti-glial fibrillary acidic protein (GFAP)	Millipore-Sigma	cat. #MAB360; RRID:AB_11212597
Rabbit polyclonal anti-glutamine synthetase (GS)	Millipore-Sigma	cat. #G2781; RRID:AB_259853
Mouse monoclonal anti-LRRC8A	Santa Cruz	cat. #sc-517113; RRID:AB_2928142
Secondary (WB): donkey anti-rabbit IgG, HRP-conjugated	GE Healthcare	cat. #NA932
Secondary (WB): sheep anti-mouse IgG, HRP-conjugated	GE Healthcare	cat #NA931
Secondary (IHC): donkey anti-mouse IgG, Alexa-Fluor 594	Thermo Fisher Scientific	cat #A32744; RRID:AB_2762826
Secondary (IHC): goat anti-mouse IgG, Alexa-Fluor 488	Thermo Fisher Scientific	cat # A32723; RRID:AB_2633275
Secondary (IHC): goat anti-rabbit IgG, Alexa-Fluor 647	Thermo Fisher Scientific	cat. #A21244; RRID:AB_2535812
Secondary (IHC): goat anti-rabbit IgG, Alexa-Fluor 488	Thermo Fisher Scientific	cat #A32731; RRID:AB_2633280
Chemicals peptides, and recombinant proteins		
d-[2,3-^{3} H]aspartate	Perkin Elmer	cat. #NET50100
Corn oil	Millipore-Sigma	cat #C8267
4-Hydroxy-tamoxifen	Millipore-Sigma	cat #H6278
Laemmeli buffer	Bio-Rad	cat. #1610737
Tamoxifen	Millipore-Sigma	cat #T5648
ProLong Glass Antifade Mountant	Thermo Fisher Scientific	cat. #P36984
Protease inhibitor cocktail	Thermo Fisher Scientific	cat. #78430
Paraformaldehyde, 4% in PBS	Santa Cruz Biotechnology	cat. #sc-281692
Restore buffer	Thermo Fisher Scientific	cat. #21059
Tissue-Tek O.C.T. compound	Sakura Finetek	cat. #4583
Critical commercial assays		
ECL reagent	GE Healthcare	cat. #RPN2232
Bicinchoninic acid assay	Thermo Fisher Scientific	cat. #23225
Deposited data		
Raw and analyzed data	This paper	Open Science Framework: https://osf.io/jnpca
Raw images, western blots	This paper	Open Science Framework: https://osf.io/jnpca
Raw images, brain infarction TTC staining	This paper	Open Science Framework: https://osf.io/jnpca
Experimental models: Organisms/strains		
Mouse (*M. musculus*), C57BL/6J	Jackson Laboratory	JAX: 000664; RRID:IMSR_JAX:000664
Mouse (*M. musculus*), C57BL/6J; *Lrrc8a*$^{fl/fl}$ (*Swell1*$^{fl/fl}$)	Shared by Dr. Rajan Sah	PMID: 28436964
Mouse (*M. musculus*), C57BL/6J B6N.FVB-Tg (Aldh1l1-cre/ERT2)1Khakh/J)	Jackson Laboratory	JAX: 031008; RRID:IMSR_JAX:031008
Mouse (*M. musculus*) C57BL/6J; B6.Cg-*Tg(Nes-cre)1*^{Kln}/J	Jackson Laboratory	JAX: 003771; RRID:IMSR_JAX:003771

(*Continued on next page*)

Continued

REAGENT or RESOURCE	SOURCE	IDENTIFIER
Mouse (*M. musculus*), C57BL/6J; *Aldh*$^{CreERT2/+}$;*Lrrc8a*$^{fl/fl}$	This study	Astrocyte-specific inducible LRRC8A knockout (aiKO)
Mouse (*M. musculus*) C57BL/6J; *Nestin*$^{Cre/+}$;*Lrrc8a*$^{fl/+}$	This study	Heterozygous deletion of LRRC8A (Het)
Mouse (*M. musculus*) C57BL/6J; *Nestin*$^{Cre/+}$;*Lrrc8a*$^{fl/fl}$	This study	Brain-specific LRRC8A knockout (bKO)
Rat (*R. norvegicus*), Sprague Dawley, male	Taconic Biosciences	NTac:SD; RRID:RGD_1566440
Software and algorithms		
ANY-maze	Stoelting Co.	RRID:SCR_014289
Neurolucida 11.03	MBF Bioscience	RRID:SCR_016788
Prism 7.0	GraphPad Software	RRID:SCR_002798

RESOURCE AVAILABILITY

Lead contact

Further information and requests for resources or reagents should be directed to and will be fulfilled by the lead contact, Alexander A. Mongin (mongina@amc.edu).

Materials availability

The work included in this study used genetically modified *Lrrc8a*$^{fl/fl}$ (*Swell1*$^{fl/fl}$) mouse, originally produced in the laboratory of the co-author Rajan Sah and used under interinstitutional material transfer agreement. All other animal resources and reagents are available from commercial sources.

Data and code availability

- All primary data used in statistical analyses and original western blot and TTC staining images are deposited and freely available at Open Science Framework: registration https://osf.io/jnpca.
- This paper did not use coding for data processing and analysis.
- Any additional information required to reanalyze the data reported in this manuscript is available from the lead contact upon request.

EXPERIMENTAL MODEL AND SUBJECT DETAILS

Ethics statement

All animal procedures used in the present study were approved by the Institutional Animal Care and Use Committee of Albany Medical College (ACUP 18-04002, 18-12001, 18-12003, 21-11002), and strictly conformed to the Guide for the Care and Use of Laboratory Animals as adopted by the U.S. National Institutes of Health, 8th edition (https://grants-nih-gov.elibrary.amc.edu/grants/olaw/Guide-for-the-Care-and-Use-of-Laboratory-Animals.pdf).

Animals

Mice were housed in a temperature, humidity, and light-controlled facility on a 12:12 h light/dark cycle and given free access to food and water. Experiments were performed in age-matched controls of both sexes, divided as evenly as possible between males and females. *Lrrc8a*$^{fl/fl}$ (*Swell1*$^{fl/fl}$) mice were generated as previously described.[72]

Astrocyte-specific, inducible *Lrrc8a* knockout mice were produced by breeding *Lrrc8a*$^{fl/fl}$ female mice with commercially available *Aldh*$^{CreERT2/+}$ male mice (B6N.FVB-Tg(Aldh1l1-cre/ERT2)1Khakh/J, Jackson Laboratory stock # 031008) both on a C57BL/6J background. After initial steps, *Aldh1l1*$^{Cre/+}$;*Lrrc8a*$^{fl/fl}$ males were crossed again with *Lrrc8a*$^{fl/fl}$ females mice to produce *Aldh1l1*$^{Cre/+}$;*Lrrc8a*$^{fl/fl}$ inducible astrocytic knockout mice and *Lrrc8a*$^{fl/fl}$ littermate controls. To activate Cre mice were treated with either tamoxifen (120 mg/kg, five daily injections) or an equal volume of vehicle (corn oil).

Brain-specific *Lrrc8a* knockout mice were produced by breeding *Lrrc8a*$^{fl/fl}$ female mice with commercially available *Nestin*$^{Cre/+}$ male mice (B6.Cg-*Tg(Nes-cre)1*^{Kln}/J; Jackson Laboratory stock #003771), both on a C57BL/6J background. *Nestin*$^{Cre/+}$;*Lrrc8a*$^{fl/+}$ heterozygous males were crossed again with *Lrrc8a*$^{fl/fl}$ female mice to produce *Nestin*$^{Cre/+}$;*Lrrc8a*$^{fl/fl}$ knockout mice, heterozygous deletion and two types of littermate controls (four genotypes in total, as shown in Figure 4A).

All genotypes were confirmed by PCR analysis across the predicted loxP insertion sites surrounding *Lrrc8a* exon 3, or for the *Aldh1l1*^{Cre} and *Nestin*$^{Cre/+}$ transgene insertion according to the Jackson Laboratory genotyping protocols.

All microdialysis studies were performed in male Sprague-Dawley rats (Taconic Farms, 230-280 g). Animals were maintained on a 12/12-h light/dark cycle and allowed free access to food and water.

METHOD DETAILS

Cell cultures of brain astrocytes

Primary cultures of mouse astrocytes were prepared from cortices of newborn (P0-P1) male and female mice. Complete litters were utilized, and tail snips of each pup were taken for genotyping. Neonates were anesthetized by cooling and rapidly decapitated. Brains were harvested in ice-cold sterile Dulbecco's phosphate-buffered saline without calcium and magnesium (ThermoFisher Scientific, cat. #14190144). Cortical tissue was dissected from meninges, minced using a sterile surgical blade, and additionally triturated by pipetting. Triturated tissue was then digested for 5 min using the recombinant protease TrypLE Express (ThermoFisher Scientific, cat. #12605) at room temperature. The dissociated cells were sedimented at 900 g for 10 minutes at 4°C. Cell pellets were resuspended in Earl's minimal essential medium (MEM) supplemented with 10% heat-inactivated horse serum (HIHS) and penicillin/streptomycin (all components from ThermoFisher Scientific/Invitrogen). To obtain an enriched astrocyte population, cells from each individual brain were separately plated onto an T75 flask pretreated with poly-d-lysine (Sigma-Millipore, cat. #P6407) and grown in a humidified atmosphere of 5% CO_2/balance air at 37°C. Cell cultures typically reached confluency around 10 days and were maintained up to six weeks until replating for functional assays. The purity of astrocyte populations was periodically verified with immunocytochemistry by staining for the astrocyte marker, glial fibrillary acidic protein (GFAP, Millipore-Sigma, 1:400), and exceeded 90%.

Processing of brain tissue samples

To collect brain tissue, mice were transcardially perfused with either PBS for western blot, or 4% paraformaldehyde in PBS for immunohistochemistry after complete anesthesia with a lethal dose of sodium pentobarbital (100 mg/kg).

For immunohistochemistry, brains were removed and additionally postfixed in 4% paraformaldehyde for 24 h, dehydrated in 15% sucrose solution for 24 h, and then in 30% sucrose solution for full cryopreservation (all steps at 4°C). Brains were attached to a cryostat specimen stage using Tissue-Tek OCT compound, allowed to freeze to −20°C and sectioned using a CM3050 cryostat (Leica, Wetzlar, Germany, RRID: SCR_016844) into 25-μm thick sections. Sections were placed into cryoprotectant media containing 30% ethylene glycol and 20% glycerol in Tris-buffered saline (TBS) and stored at −20°C until immunohistochemistry is performed.

For western blotting, brains were removed, sectioned to two hemispheres and immediately snap-frozen in liquid nitrogen. A single hemisphere was homogenized using a mechanical homogenizer (PRO200, PROScientific, Oxford, CT, USA) in a tissue lysis buffer containing 150 mM NaCl, 50 mM Tris HCl (pH 8.0), 0.1% Triton X-100, and 5% protease inhibitor cocktail. Samples were clarified by a brief centrifugation (10,000 *g* for 5minat 4°C) and the supernatants were collected and diluted with 2× reducing Laemmli buffer.

Immunohistochemistry

For immunohistochemical detection, floating sections were washed with PBS and blocked in PBS with 2% normal goat serum and 0.2% TX-100 for one hour at room temperature. They were next incubated overnight at 4°C in the same solution additionally containing mouse monoclonal anti-GFAP antibody (1:400) and rabbit polyclonal anti-glutamine synthetase antibody (1:5,000). The next morning, brain sections

were washed in PBS and incubated for 2h at room temperature with the secondary antibodies: goat anti-mouse Alexa-Fluor 488 (1:400 for GFAP) and goat anti-rabbit Alexa-Fluor 647 (1:400 for GS). After PBS wash, sections were counterstained with 0.05 μg/ml DAPI, additionally washed with PBS, and transferred onto glass slides. Slides were dried overnight at room temperature in the dark, and then mounted with ProLong Glass Antifade Mountant. Immunolabeled brain sections were scanned using a Zeiss AX10 microscope at 200× magnification, and the resulting images stitched together with Neurolucida 11.03 software. Alternatively, to determine 3D-colocalization of tdTomato reporter and astrocytic makers, images were acquired using a Zeiss LSM880 confocal microscope with a LCI Plan- Neofluar 25×/0.8 Imm Korr DIC objective (Carl Zeiss, RRID:SCR_0113672).

Western blotting analysis

The success of LRRC8A deletion was confirmed using semi-quantitative Western blot analyses in protein lysates from brain tissue and astrocyte cultures. Additionally, we quantified changes in the brain expression levels of the astrocytic glutamate transporter GLT-1. Protein lysates in the reducing Laemmli buffer were boiled for 5 min, loaded onto 10% Mini-PROTEAN TGX gels (Bio-Rad, cat #4561033), and separated according to a standard SDS-PAGE protocol. Separated proteins were electrotransferred onto a polyvinylidene difluoride membrane (PVDF, Bio-Rad, cat. #1620177). Membranes were blocked for 5 min in Tris-buffered saline containing 0.1% Tween-20 (TBS-T) and 5% milk and incubated overnight in the same blocking buffer with one of the following primary antibodies: mouse monoclonal anti-LRRC8A (Santa Cruz, dilution 1:500) rabbit polyclonal anti-GLT-1 (Abcam, dilution 1:25,000). Blots were washed (3x) with TBS-T and probed with the species-matching secondary horseradish peroxidase-conjugated antibody: donkey anti-rabbit (GE Healthcare, dilution 1:10.000) or sheep anti-mouse IgG (GE Healthcare, 1:10,000) in TBS-T containing 5% milk for 2h at room temperature. After a final wash, immunoreactivity was measured using ECL reagent (GE Healthcare, cat. #RPN2232) and visualized in a Bio-Rad ChemiDoc Imager (RRID:SCR_019684). For loading controls, membranes were re-probed with the HRP-conjugated primary anti-β-actin antibody for 20 min (Millipore-Sigma, 1:50,000), and the β-actin immunoreactivity was visualized.

VRAC activity assay

VRAC activity was quantified by measuring the release of the non-metabolizable analog of glutamate, D-[^{3}H]aspartate, as described and validated in our prior work.[36,64,81] Primary astrocyte cultures from all relevant genotypes were plated on to poly-D-lysine treated 18×18 mm glass coverslips. Cells were loaded with 2 μCi/ml D-[2,3-^{3}H]aspartate (Perkin Elmer, Waltham, MA, cat. #NET50100) in MEM +HIHS cell culture medium. Extracellular isotope was removed by washing in the chemically defined isoosmotic Basal medium containing (in mM) 135 NaCl, 3.8 KCl, 1.2 $MgSO_4$, 1.3 $CaCl_2$, 1.2 KH_2PO_4, 10 HEPES, and 10 D-glucose (pH 7.4, osmolarity 290 ±2mOsm). Coverslips were then transferred into a Leucite perfusion chamber with inlet/outlet ports. Cells were superfused with a either isoosmotic Basal medium or Hypoosmotic medium in which osmolarity was reduced to 200 ±2 mOsm (50-mM reduction in [NaCl]). One-minute perfusate fractions (~1.2 mL) were collected into scintillation vials via an automated fraction collector Spectra/Chrom CF-1 (Spectrum Chemical, New Brunswick, NJ, USA). At the end of sample collection, cell were lysed in solution of 2% sodium dodecyl sulfate (SDS) plus 8 mM EDTA. The [^{3}H] content in individual samples was determined using a TriCarb 4910 TR scintillation counter (Perkin Elmer) after addition of scintillation liquid (Ecoscint, Atlanta Biologicals, Atlanta, GA, USA, cat. #LS-273). Outcomes were analyzed and reported as fractional release ratios relative to the total [^{3}H] content for each time point, calculated using a custom Excel program.

Middle cerebral artery occlusion surgery in mice

MCAo was performed in line with published protocols[40] with minor modifications as described below. After a neck incision and dissection of left external carotid artery, a 6-0 silicon coated occlusion probe (Catalog No. 602356PK10, Doccol, Redland, CA, USA) was inserted and advanced into the internal carotid artery to block the blood flow at the origin of the middle cerebral artery. A fiberoptic cable (1-mm diameter) was glued to the exposed skull (approximately 1.5 mm caudal, 4 mm lateral of bregma) and the cerebral blood flow in the ischemic tissue was monitored in real time by laser-Doppler flowmetry (moorVMS-LDF1, Moor Instruments). Body temperature was monitored with a rectal probe in all animals and kept at 37 ±0.5°C. In this setting, brain temperature was 36.5 ±0.3°C as determined in a pilot group of mice using a probe placed in the brain. After 40-min occlusion, probe was withdrawn, and blood flow was restored. After ten minutes of reperfusion, neck incision was closed using surgical staples. Lidocaine hydrochloride jelly

(2%, Akorn) was applied topically and Bupivacaine (0.25%, Auromedics) was injected subcutaneously as local analgesics postMCAo surgery. During recovery, additional analgesia was maintained by repeated local application of 2.5% Lidocaine/2.5% Prilocaine Cream (Actavis). We applied the following preregistered criteria to verify MCAo surgery success and minimize experimental variability. The inclusion criteria were (1) average reduction of cerebral blood flow by 75% or more during occlusion (equal or below 25% of the baseline measured with laser Doppler probe); (2) restoration and stabilization of blood flow to more than 65% of the original baseline within 10 minutes after filament withdrawal. The exclusion criteria were (1) insufficient reduction of blood flow during MCAo, (2) incomplete reperfusion (below targeted level), (3) animal death during recovery from anesthesia or within 1 hour after completion of MCAo. All included animals were allowed to survive for full 72 h and euthanized after behavioral testing. The 72-h endpoint for stroke outcomes was selected to ensure that thew ischemic lesion has matured and in compliance with Stroke Therapy Academic Industry Roundtable (STAIR) recommendations (*Stroke*, 1999). Premature animal mortality between 1 and 72 h was analyzed as a secondary outcome and reported in the paper. The complete animal use in stroke experiments is reported in Figures S3–S8.

Brain lesion measurements

Ischemic lesion sizeswere quantified at 24 or 72 h after initiation of ischemia using a triphenyl tetrazolium chloride (TTC) method.[82] TTC stains viable tissue in shades of red while the infarcted tissue remains unstained. Animals were deeply anesthetized via 5% isoflurane and decapitated. Brains were extracted and sliced rostro-caudally into serial 1-mm-thick slices using a Leica VT1200S vibratome (RRID: SCR_020243). Slices were submerged into 2% TTC solution in PBS and stained for 15-30 min at room temperature in a dark. Processed tissue specimens were fixed in 4% formaldehyde and stored at 4°C until scanned. Images were captured with a digital scanner and analyzed using ImageJ software.[83] The infarct volumes were corrected for brain edema and calculated by tracing healthy tissue in the ipsilateral hemispheres and subtracting it from contralateral hemisphere areas on all sections.[84]

Evaluation of neurological deficits

While stroke lesion size can be used as a primary endpoint, there is a consensus in the field that behavioral outcomes are important as additional endpoints.[85] Accordingly, we utilized tree different behavioral assessments (Neuroscore, Open Field test, and Pole test) to assess neurological recovery.

Neurological score

MCAo animals were evaluated on a 5-point neurological score scale, immediately after recovery from anesthesia and daily until euthanasia. The scores were assigned as follows: 0, no neurological deficits; 1, failure to extend left forepaw; 2, circling to the left; 3, inability to carry bodyweight, falling to the left; 4, absence of spontaneous locomotion; 5, death.

Open field test

Changes in spontaneous locomotor activity were tested in the open field, 72 h post-surgery.[41] Briefly, mice were released into the open field chamber (40 × 40 × 40 cm) and allowed to explore freely for 10 min. A video tracking software (AnyMaze) was used to track and analyze animals walking distance, time spent in the center vs the wall zones of the apparatus and the cumulative angle of rotation during locomotion. Only total travel distance is reported here.

Pole test

This test is a simple yet sensitive assay for evaluating motor function and coordination during the early post-stroke stages.[41]Animals were trained to perform this task prior to MCAo. Ten rounds of training were generally sufficient for the test acclimation. Briefly, mice were placed on a 70-cm steel pole (1-cm thick) facing upwards and allowed to make a 180 degree turn and descend to the floor. For post-MCAo testing, the time to make a full turn (*tTurn*) and the total time to reach the floor (*tDescend*) was measured by analyzing video recordings of 5 successful trials and averaging their results. Mice that were too sick to perform (i.e., showing no spontaneous movement or repeatedly dropping from the pole) were assigned the highest scores among all the cohorts.

Middle cerebral artery occlusion surgery and microdialysis in rats

Anesthesia was induced with 5% isoflurane in 30% O_2/balance N_2 and maintained through surgical procedures with 1.75-2.25% isoflurane under constant observation. To prevent excessive fluid secretion in the

respiratory system and gastrointestinal tract, 0.4 mg/kg atropine sulfate was given via intramuscular injection. Animals were kept hydrated with hourly intraperitoneal (i.p.) injections of 1 ml physiological saline. Body and brain temperatures were maintained between 36.5°C to 37.5°C using a heating pad and measured with two probes placed rectally and in the temporalis muscle, respectively.

Two symmetrical bilateral microdialysis probes (CX-I series, 0.22×2 mm membrane, 50,000 kD molecular weight cutoff, Eicom Corporation, San Diego, CA) were lowered into the cortex through small burr holes, ~4 h before initiation of ischemia (see experimental design diagram in Figure 7). Probe placement was done using a stereotaxic frame (David Kopf Instruments, Tujunga, CA). The position of the probes was 2 mm anteroposterior, 5 mm lateral from bregma, and 2.6 mm down from dura. The contralateral microdialysis sampling was used to assure the long-term stability of neurotransmitter measurements and account for potential effects of local, probe-induced inflammation. Artificial cerebrospinal fluid (aCSF) was perfused at a flow rate of 2 μl/min throughout the experiment. The composition of aCSF was as follows (in mM): 120 NaCl, 2.7 KCl, 1 $MgSO_4$, 1.2 $CaCl_2$, 25 $NaHCO_3$, 0.05 ascorbic acid (pH=7.3). Microdialysis samples were collected every 20 min after a 1-1.5-h stabilization period using a CMA 470 refrigerated fraction collector (CMA Microdialysis, Holliston, MA). Cerebral blood flow was measured using a MoorLAB laser Doppler sensor mounted next to the microdialysis probe and acquisition module (Moor Instruments, Axminster, Devon, UK).

Middle cerebral artery occlusion (MCAo) was performed using an intraluminal suture technique as originally developed by Longa and colleagues[86] with modification detailed in our recent work.[50] Briefly, the right common carotid artery (CCA) and bifurcation of the external carotid and the internal carotid arteries (ECA and ICA) were exposed via incision on the neck. The ECA was coagulated. A standardized silicon-coated microfilament with a tip of 0.41 or 0.43 mm diameter (Doccol Corporation) was inserted via a stump of the ECA into the ICA up to 19-20 mm from the bifurcation to occlude the origin of MCA. The laser Doppler readings were used to ensure proper reduction of the blood flow rate to the levels that are expected in the ischemic penumbra. If blood flow was reduced by less than 80±1% (20% of the pre-ischemia values), animals were excluded from analysis on the basis of incomplete ischemia. After completion of ischemia and reperfusion in microdialysis experiments animals were euthanized with an overdose of sodium pentobarbital.

Analysis of microdialysate samples

Microdialysate samples were analyzed off-line. Amino acid levels in each sample were determined by a reverse-phase HPLC using an Agilent 1200 HPLC setup and Eclipse XDB-C18 column (both from Agilent Technologies, Santa Clara, CA). Precolumn derivatization was performed with a freshly prepared mix of o-phthalaldehyde and 2-mercaptoethanol in 0.4 M sodium tetraborate buffer (pH = 9.5). The amino acid derivatives were eluted with solvent containing 30 mM NaH_2PO_4, 1% tetrahydrofuran, 30 mM sodium acetate, 0.05% sodium azide, and increasing concentration of HPLC grade methanol (10–30%). Fluorescence signal was measured using a programmable 1200 series fluorescence detector (Agilent). Amino acid standards (L-aspartate, L-glutamate, and taurine), were processed in the same fashion and used to identify amino acid peaks and calculate concentrations of individual amino acids in the samples.

QUANTIFICATION AND STATISTICAL ANALYSIS

Experimental outcomes in different genotypes have been statistically compared using one-way (effect of genotype) or two-way (effect of genotype and treatment) ANOVA with the Tukey or Sidak post-hoc tests for multiple comparisons, as appropriate. The effects of sex were not included in the main analysis but were additionally evaluated in a separate post-hoc assessment. For results involving multiple measurements, we used the repeated measures ANOVA or mixed model (Geisser-Greenhouse correction) with the Sidak's posthoc test. Mortality values were evaluated using a Log-rank (Mantel-Cox) test. All statistical comparisons were performed using Prism 9.0 software (GraphPad Software Inc., La Jolla, CA). P values <0.05 were considered statistically significant.

The design of animal experiments was preplanned, including primary and secondary outcomes, and preregistered with the Open Science Framework (https://osf.io/46npj and https://osf.io/3s7ab). The initial assumption was that nine animals per group would be sufficient to yield 80% power assuming that the maximal difference between groups will be at least 1.66 times the within group standard deviation (assumptions: alpha=0.05; parametric ANOVA; one factor, 4 levels; computed using Minitab software). This

number (9/group) was further inflated to 15 mice/group based on the following assumptions. We expected ~10% surgical mortality, ~15% attrition based on stroke exclusion criteria, and additional ~15% mortality due to tamoxifen toxicity. As study progressed, we found that that some of the assumptions would have to be modified because we have higher-than-expected surgical attrition and stroke mortality. Also, bLRRC8A KO mice have an inherited seizure phenotype, making it difficult to produce equal number of contemporary surgeries in each group. For these reasons we have completed stroke experiments when the histological testing of primary outcomes was $\geq$9 mice per group.